

A Goodput Distribution Model for Planning IEEE 802.11 WBNs in Built Environments

Ying Qu*, Bryan Ng, Michael Homer

School of Engineering and Computer Science, Victoria University of Wellington, Cotton Building, Gate 6, Kelburn Parade, Wellington, New Zealand 6140

Abstract

IEEE 802.11 wireless backhaul networks (WBNs) have emerged as a practical solution for bridging access points and backbone networks with low cost and ease of installation. However, the IEEE 802.11 protocol operates in the unlicensed spectrum and experiences unregulated interference, making it difficult to guarantee quality of service (QoS). With newer and farther reaching applications being densely deployed in built environments [1], such as small cell cellular networks and smart grids, users are increasingly expecting high QoS and fair access. This increased expectation for high QoS motivates the study of goodput models for planning IEEE 802.11 WBNs in built environments. In this paper, we design a goodput distribution model with consideration of structured placement of WBN nodes in built environments and validate our goodput model through simulations. The results show that our model provides an accurate prediction of goodput distribution in IEEE 802.11 WBNs under different traffic demands and radio propagation conditions. Such a goodput model is useful for node placement and optimising routing and channel assignment algorithms in IEEE 802.11 WBNs.

Keywords: Wireless backhaul networks, Built environments, Goodput modelling, Network planning

*corresponding author

Email addresses: `ying.qu@ecs.vuw.ac.nz` (Ying Qu), `bryan.ng@ecs.vuw.ac.nz` (Bryan Ng), `michael.homer@ecs.vuw.ac.nz` (Michael Homer)

1. Introduction

With the rapid development of data-hungry applications and increasing growth of traffic data, wireless networks are evolving to improve network performance [2]. For example, to expand conventional cellular architectures, an efficient approach is to combine macro-cell networks with small-cell networks. Small-cell networks provide coverage at some blind spots with the advantage of low cost and easy installation [3].

These small-cell networks are deployed closer to end users to improve spatial utilisation and coverage e.g. in built environments such as residential areas, subways, and offices [3]. Such built environments are typically densely populated and have a highly structured and regular topology such as a line or a grid topology (see Figure 1).

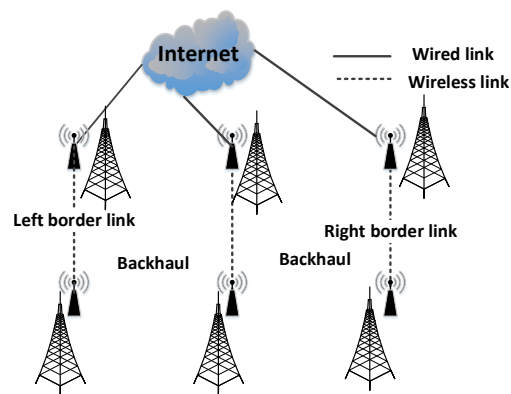


Figure 1: Illustration of a P2P wireless backhaul network in a linear layout

In built environments, wireless backhaul networks (WBNs) have emerged as a practical solution for bridging small cell networks and backbone networks in lieu of wired backhaul networks when it is difficult to install new wired links [4, 5]. The IEEE 802.11 is a popular protocol used by WBNs due to cost-efficient deployment, flexible and easy installation, especially when an operator has limited budget for the use of dedicated microwave links, satellite, and WiMax [2, 6].

20 However, poor performance in WBNs based on the IEEE 802.11 wireless in-
frastructure has caught researchers' attention [7, 8]. For the IEEE 802.11 proto-
col to efficiently support WBNs, some performance issues such as throughput
degradation and fairness must first be resolved [6, 9–11]. In broadcast chan-
nels, such as the one used in IEEE 802.11, flow starvation appears to be caused
25 by the so-called "border effect", which refers to the border links dominating
the transmission in a WBN [12] (see Figure 1). Such border effect causes severe
unfairness and significantly degrades the QoS. These issues prompt investi-
gations into the root cause of some severe performance issues such as flow
starvation.

30 Some of the performance issues with using the IEEE 802.11 protocol in
WBNs can be traced back to poor network planning [13] (See Section 2.1 for
more details). One weakness of existing network planning in IEEE 802.11
WBNs is that these planning strategies mainly focus on maintaining cover-
age within some budget constraints [14]. Such planning strategies may fail
35 to support QoS requirements for newfound uses such as smart grids [15, 16] or
small-cell backhubs [3] because the reduced capacity may be due to the node
placement of a WBN (topology). Another weakness of network planning in
WBNs is that existing models are not designed specifically for guiding the de-
ployment in built environments. Hence, an opportunity exists to shed light on
40 WBN planning through a new goodput model to accurately predict the link
quality in IEEE 802.11 WBNs.

 In our previous work, we have studied the carrier sensing effect on good-
put pattern in IEEE 802.11 WBNs, whereby carrier sensing refers to the Carrier
Sense Multiple Access with Collision Avoidance (CSMA/CA) medium ac-
45 cess control (MAC) protocol [17]. This carrier sensing mechanism controls the
media access in IEEE 802.11 WBNs that directly determines the network per-
formance. In [18], we found a four-phase goodput pattern in a two-link WBN
representing an effective carrier sensing scenario, where all nodes are either
within each other's carrier sensing range or out of each other's carrier sensing
50 range. We also proposed a goodput distribution model to extend the study

in [18] to ineffective carrier sensing scenarios, where not all nodes are within each other's carrier sensing range. The proposed goodput distribution model can provide accurate prediction of goodput using the saturated traffic assumption for ineffective carrier sensing scenarios in [19].

55 In this study, we further extend our previous work from two aspects. First, we use a unified goodput model covering effective and ineffective carrier sensing. Moreover, this new model is flexible for both saturated and unsaturated traffic demands. Second, we validate the proposed model with two different radio propagation models relevant to the operation of WBNs in built environ-
60 ments. The outcomes from the research in this paper help network planners accurately predict the goodput distribution with a given topology in IEEE 802.11 WBNs.

In this paper, we detail the development of a goodput model for IEEE 802.11 WBNs as a three step process. Our first step is to characterize the poor fit of
65 the disk-graph models that have been widely used in performance modelling in IEEE 802.11 WBNs. Then, based on these observations, we develop a goodput distribution model to predict link level goodput based on network topology and traffic demands. Finally, we validate this model through simulations under different traffic demands and different radio propagation models that
70 reflect typical built environments.

The rest of this paper is organised as follows. Section 2 summarises related work and motivates the need for developing a goodput model for IEEE 802.11 WBNs. Section 3 presents the goodput pattern observed in an IEEE 802.11 WBN and Section 4 explains the derivation of our goodput model. Sections 5
75 and 6 validate the model under two different propagation models followed by the conclusion in Section 7.

2. Related work

In this section, we first describe the problem of planning IEEE 802.11 WBNs in built environments and then discuss the shortcomings of existing goodput

80 models in planning WBNs. Note that WBNs refers to WBNs using the IEEE 802.11 protocol for the rest of this paper.

2.1. *Planning WBNs in built environments*

In built environments, WBN planning involves examining highly structured topologies such as a line or a grid topology. The grid topology naturally occurs in scenarios such as transportation system (roads, railway tracks) and urban living spaces (residential areas, buildings and power grid). Several studies demonstrated that the performance of a WBN is largely determined by its topology and that grid placement outperforms arbitrary placement in terms of coverage, connectivity, and fair capacity allocation [20, 21]. Given the highly structured layout of built environments, investigating WBN planning to achieve a certain level of QoS makes for a more interesting and realistic study to satisfy various applications.

Network planning for IEEE 802.11 WBNs has received very little attention compared with other wireless networks such as 3G cellular network [22–24]. It borrows strategies from other types of wireless network due to cost constraint and the operation in unregulated spectrum [3, 25, 26]. However, performance issues in IEEE 802.11 WBNs show that the strategies from other networks may not be suitable for planning IEEE 802.11 WBNs due to the differences in the medium access control (MAC) protocol in use [7]. Current practice of ad hoc placement of nodes in IEEE 802.11 WBNs may be able to improve the coverage but this strategy no longer suffices for the requirements of QoS in dense environments, such as networking in smart grids and intelligent transport systems [27]. In indoor placement of wireless local area network (WLAN), introducing a new access point may improve the wireless coverage and overall goodput [28]. However, adding a new access point does not necessarily translate to better fairness because the new access point introduces additional contention or perhaps may cause severe unfairness like flow starvation [29]. Therefore, the strategies from other networks are not suitable for planning IEEE 802.11 WBNs and thus it needs to further improve the planning to pro-

110 **vide better goodput and fairness.**

Generally, flow starvation results from the border effect attributable to node placement that is determined at the network planning stage. Because the border links only have neighbouring links on one side (see Figure 1), these border links experience less channel contention and are more likely to transmit
115 more packets than the middle links in between border links. Middle links have neighbouring links on both sides and thus some middle links between the border links may experience extremely low throughput (what is commonly called flow starvation). Such flow starvation significantly impacts network QoS and users' experience.

120 These above issues have spawned a renewed interest in improving IEEE 802.11 WBN planning with better performance. To address these issues, a mathematical model is essential for planning and optimising IEEE 802.11 WBNs. A goodput model representing IEEE 802.11 protocols will be convenient for analysing the performance problems in IEEE 802.11 WBNs and improving pro-
125 tocol designs [30].

Next, we will discuss about selecting a suitable goodput model to help network designer predict the potential network performance before deployment.

2.2. *Goodput models in WBNs*

**A suitable goodput model is crucial for planning IEEE 802.11 WBNs be-
130 cause such a model abstracts the essence of the network such as the behaviour of wireless links and shows the interrelationships between key factors. Network planners use a goodput model to improve planning by predicting network performance before deploying the network. Note that in this paper goodput is used interchangeably with throughput. Since a goodput model for plan-
135 ning IEEE 802.11 WBNs normally involves topology, carrier sensing mechanism, and traffic demand, we will review how existing goodput models consider topology, carrier sensing scenario, and traffic demand separately.**

2.2.1. Goodput models with structured topology in built environments

First, a goodput model should consider topology because network performance directly relates to the placement of nodes in WBNs [20, 31]. Moreover, at the planning stage, the number of nodes and the location of these nodes in a WBN are known. Hence, these information should be considered in this goodput model for better accuracy.

The recent developments in WBNs have been closely linked to the emergence of small-cell networks which are typically deployed in a highly structured topology such as a line or a grid topology. Our previous work in [18, 19] demonstrated that existing goodput models do not explicitly take into account the geometries of a structured topology which leads to inaccuracies in goodput prediction. Several studies have developed goodput models with consideration of network topology [29, 32–34]. However, none of these goodput distribution models focus on planning a WBN in a highly structured built environment. Therefore, we want to develop a goodput model tailored to a structured topology, which is desirable for WBN planning in built environments.

2.2.2. Goodput models with effective and ineffective carrier sensing using IEEE 802.11

For planning purposes, a goodput model needs to be generalized for various scenarios in WBNs. In this paper, we focus on studying the IEEE 802.11 media access control (MAC) protocols because the goodput in WBNs relies heavily on the efficiency of the carrier sensing mechanism. The IEEE 802.11 carrier sensing mechanism is designed to protect packet transmission under effective carrier sensing. However, ineffective carrier sensing scenarios such as exposed nodes and hidden nodes are still common in real-world applications of WBNs [35–37]. Therefore, a goodput model needs to consider both effective and ineffective carrier sensing scenarios.

A broad class of goodput models for IEEE 802.11 protocol under effective carrier sensing is based on the disk-graph model [38] that has been widely used in modelling carrier sensing mechanism for decades [39, 40]. Such a disk-graph model is a pairwise model in that the interference between two nodes is

determined by the distance between the two nodes. The disk in the disk-graph model can be regarded as the interference range of a given node. When two nodes are within each other's disk, they interfere with each other while when they are out of each other's disk, no interference exists between them.

The disk-graph model can be traced back to Bianchi's models [41, 42] and Cali's model [43] characterising goodput under effective carrier sensing conditions. Both Bianchi's and Cali's models are based on single-hop wireless networks. They found that throughput of the IEEE 802.11 WLAN is related to the number of active nodes and minimum contention window size. Felemban *et al.* [44] refined Bianchi's model by considering channel state during the back-off period. Several others [45–47] extended Bianchi's model using IEEE 802.11 [17]. For these goodput models under the effective carrier sensing condition, they assumed that all nodes can share the channel capacity equally as they can all sense the signal from each other clearly. The goodput depends on the number of active nodes and the configuration parameters of CSMA.

For ineffective carrier sensing scenarios, several studies have developed goodput models with consideration of exposed nodes, hidden nodes, and border effect [48–54]. Some findings under the ineffective carrier sensing condition come to a similar conclusion to those findings from models under the effective carrier sensing condition i.e. goodput depends on the number of active nodes and the configuration parameters of CSMA. Even though these goodput models are designed for ineffective carrier sensing scenarios, they did not consider the structured topology explicitly rendering these models less useful for planning the deployment of WBNs in built environments.

Within the same area of studying ineffective carrier sensing scenarios, some studies about goodput model considered topology in their models. These models express throughput of a given link as a proportion of the probability of a successful transmission [8, 29, 32–34, 55–57]. The probability of successful transmission for a given link depends on many relevant probabilities such as the probabilities of packet arrival of its neighbouring nodes. These studies introduce many unknown probabilities related to channel state and transmis-

sion, such as collision probability, access attempt probability, leading to very
200 high computation complexity. Hence, it is difficult to apply these models to
planning WBNs.

Even though many goodput models have been studied for IEEE 802.11
MAC protocols, none of these goodput models is suitable for planning WBNs
in built environments. First, the disk-graph model is simple and easy to use but
205 many studies pointed out that disk-graph model is not accurate because this
model defines the carrier sensing effect as a binary function of distance [58, 59].
This apparent binary outcome of the carrier sensing mechanism overly simpli-
fies the interaction among neighbouring nodes so this disk-graph model can-
not accurately reflect the actual behaviour of wireless links. Moreover, disk-
210 graph model cannot explain the goodput pattern in ineffective carrier sensing
scenarios with exposed nodes, hidden nodes, and border effect. Hence, the
disk-graph model is not suitable for planning WBNs.

Second, those models for ineffective carrier sensing scenarios are also not
suitable for network planning as they either do not consider the structured
215 topology or made unrealistic assumptions that all detailed flow level informa-
tion is known in advance. At the network planning stage, it is not realistic to
collect flow level information and also difficult to apply these models to net-
work planning. Therefore, a simple goodput distribution model tailored to a
structured topology is desirable to plan a WBN in the built environment with
220 better QoS.

2.2.3. *Goodput models considering traffic demand*

Traffic demand is also a key factor for a goodput model because this model
must be generalisable to deal with various application requirements at net-
work planning stage. In addition, the desired goodput model should provide
225 a goodput distribution because goodput distribution can comprehensively re-
flect network performance. Saturated traffic demand has been used in Bianchi's
models [41, 42] and Cali's model [43] to simplify the analysis. To generalise
the goodput model, other studies extended their studies with both saturated

and unsaturated traffic demands [45–47]. However, the studies about goodput
230 model with both saturated and unsaturated traffic demands did not consider
both topology and effective and ineffective carrier sensing.

Since traffic demand in real-world applications varies across different do-
mains, it would be desirable for a goodput model to be flexible with both types
of demands. We aim to develop a goodput model that is flexible for both satu-
235 rated and unsaturated traffic demand with other key factors.

2.3. *Summary*

Network planning in WBNs plays an increasingly important role in ensur-
ing QoS for heterogeneous services with increasing data demands. Simplicity,
usability and accuracy of a goodput model are three elements common to a
240 successful model for network planning. The accuracy of a goodput model in
WBNs is related to the three key factors we discussed before (structured topol-
ogy, effective and ineffective carrier sensing, and traffic demand).

From our survey of the literature, we find that no goodput model has been
studied specifically for planning a WBN in highly structured built environ-
245 ments. Specifically, existing studies do not link the goodput model with three
key factors we discussed before (structured topology, effective and ineffective
carrier sensing, and traffic demand). Moreover, they do not provide insights to
network wide performance – i.e. the performance is evaluated on a single link
or adjacent links only.

250 Among the above goodput models we discussed, the disk-graph model is
the simplest model but we will show in the next section that the disk-graph
model is not suitable for planning WBNs in built environments due to the inac-
curacy. Our end goal is to develop a simple and accurate goodput distribution
model for planning WBNs (a metric that reflects network-wide performance)
255 with consideration of a structured topology for various application scenarios.

3. WBN goodput patterns with effective vs. ineffective carrier sensing

This section investigates goodput patterns through simulation in an IEEE 802.11 WBN and discusses the difference between simulation results and expectations from the disk-graph model under effective and ineffective carrier sensing scenarios. Among the goodput models discussed in section 2, the disk-graph model [38] is the simplest model that has been widely used in performance modelling in IEEE 802.11 WBNs [39, 40]. The investigation aims to identify how the disk-graph model reflects the behaviour of wireless links in IEEE 802.11 WBNs.

3.1. Simulation configurations

To characterise the difference of goodput between disk-graph model and simulation, we select two typical carrier sensing scenarios with structured linear topology and two types of traffic demands.

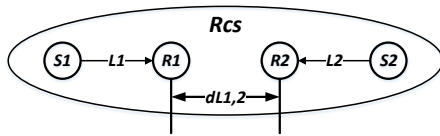


Figure 2: The two-link scenario representing effective CSMA when 2 links are within each other's carrier sensing range

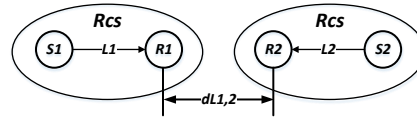


Figure 3: The two-link scenario representing effective CSMA when 2 links are out of each other's carrier sensing range

Two typical carrier sensing scenarios include effective and ineffective carrier sensing scenarios. The effective carrier sensing scenario is selected with a two-link scenario (see Figures 2 and 3), which is a building block of any WBNs. In Figure 2, four nodes $S1$, $R1$, $S2$, and $R2$ are within each other's carrier sensing range. In Figure 3, two links $L1$ and $L2$ are within each other's carrier sensing range. The ineffective carrier sensing scenario is selected with a three-link scenario (see Figure 4) that can be regarded as the combination of three two-link scenarios and includes many typical issues in WBNs such as exposed nodes, hidden nodes, and border effect.

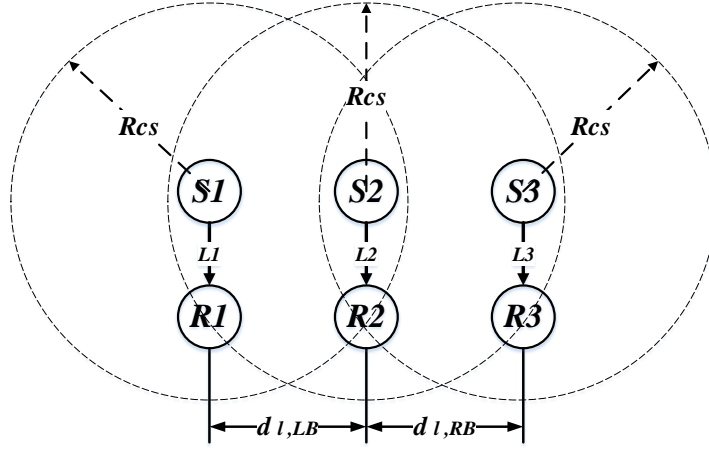


Figure 4: The three-link scenario representing ineffective CSMA with exposed nodes, hidden nodes and border effect

Two types of traffic demands considered in this paper refer to saturated and unsaturated traffic demands. Saturated traffic represents heavy traffic across the WBN (e.g. dense urban area, providing Internet access via WBNs) and unsaturated traffic represents the intermediate and light traffic across the WBN (e.g. sensor network information exchange, machine-to-machine communication and traffic from the Internet of Things). With these two scenarios and two traffic demands, we try to cover the characteristics of various application scenarios in WBNs.

All the simulations are conducted in QualNet 5.2. Table 1 lists the main configuration parameters. Note that in this paper, we only discuss physical carrier sensing (PCS) without using virtual carrier sensing.

The theoretical maximum transmission range D_{tr}^{\max} in this simulation is approximately 58 m. This value is calculated by QualNet's radio range utility with the simulation scenario as input. Moreover, in this paper, physical carrier sensing range R_{cs} is defined by a triplet consisting of (i) the minimum receiver sensitivity of -69 dBm, (ii) maximum transmission power of 16 dBm (based on Alcatel Lucent WaveLAN card), and (iii) the two-ray propagation model, which yields the distance of 435 m.

Part of the results in the following subsections appears in our previous work [18, 19]. Simulation results shown in this section are averages from 100 randomly seeded simulation runs. All averages shown are reported with confidence interval of 95% with the range from 0.9 to 9.8 kbps under the assumption that the averages are normally distributed.

Table 1: Simulation configuration parameters

Parameter Name	Value
Transmission Power	16 dBm
Receiver Sensitivity	-69 dBm
Path Loss Model	Two-Ray
Shadowing and Fading Model	None
Physical Layer	IEEE 802.11 a
Data Rate	48 Mbps
MAC Layer	PCS
Routing	Static Routing
Transportation Layer	UDP
Packet Size	1500 Bytes
Inter-packet Interval for Saturated Traffic	0.25 ms
Inter-packet Interval for Unsaturated Traffic	0.5–4.5 ms

Next, we will discuss the simulation results and how the results match up with the predictions from the disk-graph model under effective and ineffective carrier sensing conditions separately.

3.2. A disk-graph model accurately characterizes goodput distribution under effective carrier sensing in WBNs

In this subsection, we show that the disk-graph model accurately characterizes goodput distribution in effective carrier sensing by using the simulation results in a two-link scenario. The two-link scenario is a simple single-radio single-channel WBN scenario (see Figures 2 and 3). There are two pairs of nodes denoted by $(S1, R1)$ and $(S2, R2)$ in the network and communicating pairs are connected through wireless links $L1$ and $L2$ respectively. A constant

bit rate (CBR) traffic generator sending packets at 48 Mbps encapsulated with UDP is chosen as the application for the senders. All nodes are configured with identical parameters and wireless links $L1$ and $L2$ utilize the same channel.

315 For the effective carrier sensing scenario in the two-link topology, two links $L1$ and $L2$ are either within each other's carrier sensing range or out of each other's carrier sensing range. As links $L1$ and $L2$ are like "mirror" links in the two-link scenario, we will discuss the aggregated goodput of links $L1$ and $L2$ with saturated and unsaturated traffic demands.

320 3.2.1. Saturated traffic demand

In our previous paper [18], we studied the two-link scenario with saturated traffic demand and reported: (i) For distance $D_{tr} = 20\text{ m} < 0.5D_{tr}^{\max}$, very few collisions occur; (ii) when two links are within each other's carrier sensing range, they share channel capacity equally; (iii) when two links are out of each other's carrier sensing range, they appear as two separate networks.

325

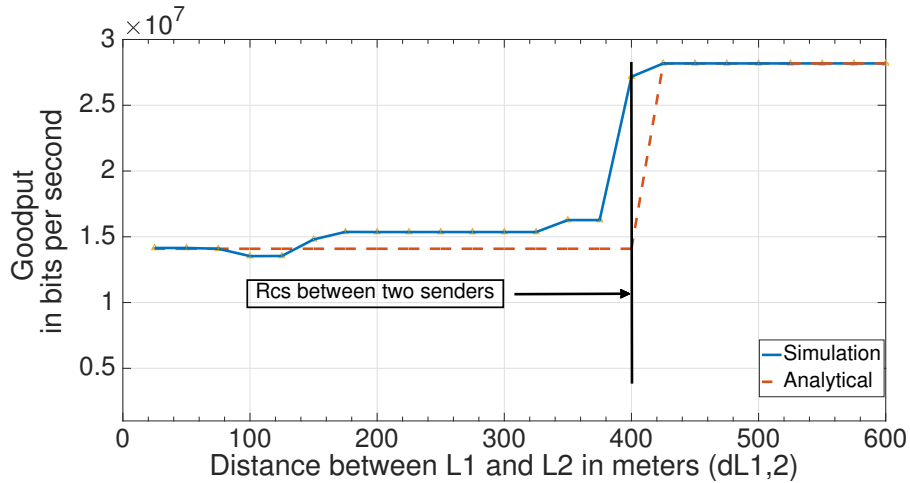


Figure 5: Comparison of aggregated goodput between simulation and disk-graph model for $D_{tr} = 20\text{ m}$ (PCS mechanism)

We show an example that uses PCS mechanism to help readers understand the above findings in Figure 5. PCS mechanism refers to physical carrier sensing mechanism without using virtual carrier sensing mechanism. In Figure 5,

the X axis refers to the distance between two links $L1$ and $L2$ denoted by $d_{L1,2}$ (see Figure 2) and Y axis presents the aggregated goodput of links $L1$ and $L2$. The two lines in the figure refer to the simulation result and the expectation from disk-graph analytical model.

The expectation from disk-graph analytical model is that within carrier sensing range, two links $L1$ and $L2$ share the channel capacity equally. Out of each other's carrier sensing range, two links $L1$ and $L2$ occupy the channel capacity. The aggregated goodput over a range of $d_{L1,2}$ shows two distinct trends in Figure 5, a step-like goodput response is observed with increasing $d_{L1,2}$. The simulation results generally match with the expected goodput pattern from disk-graph model. We notice that the simulation results are slightly higher than the prediction from the analytical model. It implies that even all nodes are within each other's carrier sensing range, carrier sensing mechanism may allow concurrent transmissions for a short term that leads to a slightly higher goodput in the simulation than the analytical prediction.

3.2.2. Unsaturated traffic demand

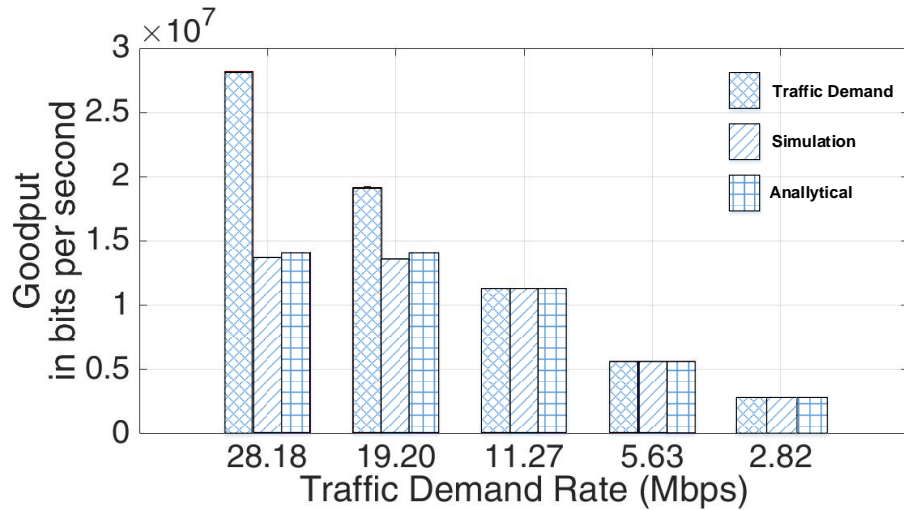


Figure 6: Comparison of aggregated goodput between simulation and disk-graph model with unsaturated traffic demands for $d_{L1,2} = 100 m$ in two-link scenario

345 For using unsaturated traffic demand in two-link scenario, we focus on the
goodput pattern when the two links are within each other's carrier sensing
range. Hence, we use the topology in Figure 2, where the distance between
links $L1$ and $L2$, $d_{L1,2} = 100m$. We select five traffic demands for links $L1$ and
 $L2$, 28.18Mbps, 19.20Mbps, 11.27Mbps, 5.63Mbps, and 2.82Mbps calculated
350 at application layer. These five traffic demands are less than 28.8Mbps that is
the net capacity excluded overhead. We compare the traffic demands (plotted
as red bars) with the actual aggregated goodput of links $L1$ and $L2$ (plotted as
blue bars) and the analytical result from the disk-graph model (plotted as pink
bars) in Figure 6.

355 The expectation of the disk-graph model is that when the sum of the traf-
fic demands of two links exceeds the net capacity, they will share the capacity
equally, while two links can achieve the desired goodput if the sum of the traf-
fic demands on both of them are less than the net capacity. These simulation
results match with the expectation from the disk-graph model.

360 In Figure 6, we find when the sum of the traffic demands of these two links
 $L1$ and $L2$ exceeds the channel capacity, both links cannot achieve their traffic
demands and have to share the channel capacity fairly (see 28.18Mbps and
19.20Mbps in Figure 6). For example, when the traffic demand rate of links
 $L1$ and $L2$ is 19.2Mbps, the sum of the traffic demand of these two links is
365 38.4Mbps that exceeds the net capacity. Because links $L1$ and $L2$ are within
each other's carrier sensing range, each link has to share the channel capacity
and can only achieve about 14Mbps goodput.

When the sum of the traffic demands of these two links is less than the net
channel capacity 28.8Mbps (see 11.27Mbps, 5.63Mbps, and 2.82Mbps in Fig-
370 ure 6), each link achieves their traffic demands. For example, when the traffic
demand rate of links $L1$ and $L2$ is 5.63Mbps, the sum of the traffic demand of
these two links is 11.26Mbps that is less than the net capacity and both links
can achieve their traffic demands.

3.3. *A disk-graph model fails to characterize goodput distribution in ineffective carrier sensing in WBNs*

375

In this subsection, we will discuss the disk-graph model fails to characterize the goodput distribution in ineffective carrier sensing scenario. We change the effective carrier sensing scenario into the ineffective carrier sensing scenario by adding a third link to the two-link scenario (see Figure 4). This scenario is a typical example for border effect where links $L1$ and $L3$ are the two border links that are beyond each other's carrier sensing range. Link $L2$ is in the middle and within the carrier sensing range of both links $L1$ and $L3$.

380

3.3.1. *Saturated traffic demand*

For saturated traffic demand in ineffective carrier sensing scenario, we reported in our previous paper [19] that when the distance between two border links exceeds each other's carrier sensing range, border effect exists and causes starvation.

385

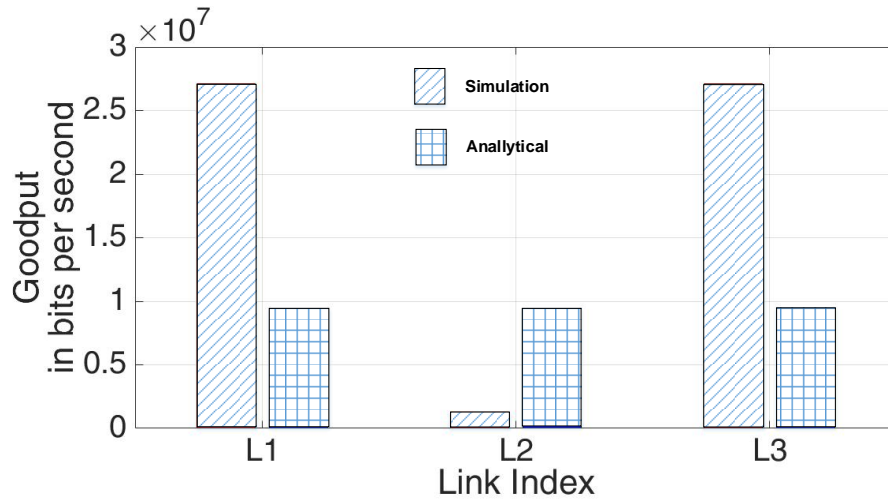


Figure 7: Comparison of goodput between simulation and disk-graph model in three-link Scenario $D = 600m$ with saturated traffic demands

We use Figure 7 as an example to explain border effect and flow starvation in which the disk-graph model fails to characterize the goodput pattern. In the

390 three link scenario (see Figure 4), as links $L1$ and $L3$ are out of each other's carrier sensing range, they do not interfere with each other. Two pairs of links $L1$ and $L2$, links $L2$ and $L3$ are still within each other's carrier sensing range. From the perspective of link $L2$, links $L1$ and $L3$ are with its carrier sensing range.

395 According to the disk-graph model, the expectation is that three links will share the channel capacity equally from the perspective of link $L2$ (see Figure 7). However, the simulation results show a different pattern in that two border links $L1$ and $L3$ utilize the spatial resource to achieve highest goodput based on the sacrifice of the middle link $L2$. These results do not match with
 400 the expected goodput pattern from the disk-graph model.

3.3.2. Unsaturated traffic demand

For unsaturated traffic demand in the three link scenario, we select five traffic demands for the links $L1$, $L2$ and $L3$, 28.18 Mbps, 19.2 Mbps, 11.27 Mbps, 5.63 Mbps, and 2.82 Mbps, which are lower than the net capacity 28.8 Mbps.

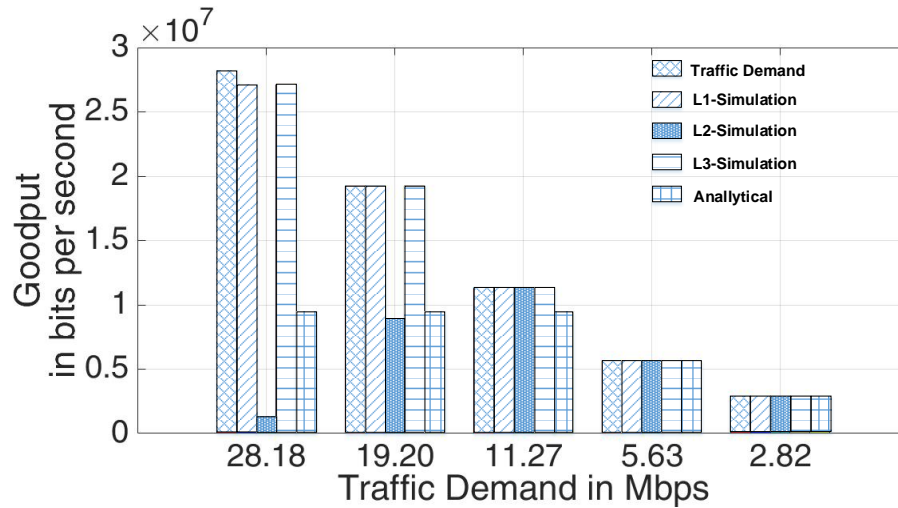


Figure 8: Comparison of goodput between simulation and disk-graph model in three-link scenario $D = 600m$ with unsaturated traffic demands

405 We list the comparison between traffic demands and the actual goodput of

three links $L1$, $L2$ and $L3$ in Figure 8. The X axis denotes the traffic demand rate of each link, the red bar represents the traffic demand rate and the blue, brown, and pink bars represent the actual goodput of the links $L1$, $L2$ and $L3$ respectively. The yellow bar refers to the prediction from the disk-graph analytical model.

The expectation of the disk-graph model is that three links will share the channel capacity from the perspective of the middle link $L2$. Therefore, when the sum of the traffic demands of the three links exceed the net capacity, these three links will share the capacity equally. If the sum of the traffic demands of the three links is less than the net capacity, these links achieve the desired goodput.

In Figure 8, we find that simulation results do not totally match with the prediction from the disk-graph model. When the sum of the traffic demands of two border links $L1$ and $L3$ exceeds the channel capacity (see 28.18 Mbps and 19.20 Mbps), starvation exists at link $L2$ and two border links $L1$ and $L3$ occupy the channel capacity. For example, when the traffic demand rate of three links is 19.2 Mbps, the sum of the traffic demand of any pair of links is 38.4 Mbps that exceeds the net capacity. The two border links $L1$ and $L3$ achieve the desired goodput while the middle link $L2$ achieves very little goodput. These goodput patterns are unexpected from the disk-graph model.

When the sum of the traffic demands of the two border links $L1$ and $L3$ is less than the channel capacity (see 11.27 Mbps, 5.63 Mbps, and 2.82 Mbps in Figure 8), starvation does not exist and these three links achieve the traffic demand. The simulation results of three links with traffic demand as 11.27 Mbps exceeds the analytical result. It implies that links $L1$ and $L3$ may transmit at the same time and channel reuse exists. The simulation results in 5.63 Mbps, and 2.82 Mbps match the expectation from the disk-graph model.

3.4. Summary

Based on the above observations, the goodput patterns in effective carrier sensing scenarios match with the expectations from the disk-graph model.

When all nodes are within each other's carrier sensing range, these nodes share the channel capacity fairly. When all nodes are out of each other's carrier sensing range, each node occupies the whole channel capacity.

However, some simulation results in ineffective carrier sensing scenarios show an unexpected goodput pattern from the disk-graph model. According to the disk-graph model, links within the carrier sensing range of a link should share channel capacity equally and the sum of goodput of the links in any interference set is below 1. However, this conclusion does not hold in the scenarios with flow starvation. Hence, the disk-graph model cannot explain the flow starvation in the middle link and the interaction between border links and middle link.

In a larger network, the main reason for unfairness between border links and middle links is that the border links and the middle links sense the channel state differently due to the layout of WBNs and carrier sensing mechanism. The border links have fewer neighbouring links than the links between borders and they are likely to transmit more packets. The transmission attempt of links in the middle have to contend with the border links and are more likely to back off until the channel is released by the border links. Therefore, this asymmetric back off leads to unfair sharing of channel among the links in WBNs and some middle links may starve.

In all, the disk-graph model is a simple model that predicts the goodput pattern in effective carrier sensing scenarios but it fails to predict the goodput pattern in ineffective carrier sensing scenarios. Next, we will develop a goodput distribution model that conserves the disk-graph model for effective carrier sensing scenarios and also extends to the unexpected goodput pattern in ineffective carrier sensing scenarios.

4. A unified goodput distribution model formulation

Based on the observation in Section 3, we will develop a unified goodput distribution model for planning WBNs in built environments. This unified

465 goodput distribution model takes both effective and ineffective carrier sensing scenarios based on structured topology into account, and it will be flexible for both saturated and unsaturated traffic demands. We define several variables to facilitate the discussion. The symbols for these variables together appear with a brief explanation in Table 2.

Table 2: Notation: symbols and their meanings.

Symbol	Explanation
E	Complete set of links in a WBN
N	The number of links in the set of E
R_{cs}	Carrier sensing range
D_{tr}^{\max}	Maximum transmission range
D_{tr}	The distance between the sender and receiver in a link
$\bar{I}\mathcal{S}(i)$	The independent set: the links out of R_{cs} of a given link i
$\bar{\gamma}(i)$	The conflict set: the links within R_{cs} of a given link i
$\chi(i)$	The number of links in the $\bar{I}\mathcal{S}(i)$
$d_{s,s}$	The distance between senders in two links
$d_{s,r}$	The distance between sender and receiver in two links
$d_{l,LB}$	The distance between a link l and the left border link LB
$d_{l,RB}$	The distance between a link l and the right border link RB
GCS_{LB}	The left border-link set in E
GCS_{RB}	The right border-link set in E
GCS'_{LB}	The dominant left border-link set in E
GCS'_{RB}	The dominant right border-link set in E
GCS_{ML}	The middle-link set in E
D	The distance between two border links in a WBN
d	The inter-link distance interval
$f(i)$	The normalized traffic demand of a link i
$G(i)$	The estimate of goodput for a link i in effective CSMA
$G_O(i)$	The optimistic estimate of goodput for a link i in ineffective CSMA
$G_P(i)$	The pessimistic estimate of goodput for a link i in ineffective CSMA
α	The starvation factor for flow starvation

470 Next, we will explain the proposed goodput distribution model with saturated and unsaturated traffic demands separately. To help understand our

model, we will provide examples to explain how to use this model to calculate the goodput distribution with a given topology and traffic demand.

4.1. A goodput distribution model for saturated traffic demand

475 The formulation for goodput model with saturated traffic is based on our previous work [18]. First, we list the assumptions for the model with saturated traffic demand as follows:

Assumption 1. *All nodes are configured with identical parameters and saturated traffic is assumed.*

480 **Assumption 2.** *A single-channel single-radio WBN is configured with a linear uniform and symmetric topology.*

Assumption 3. *The propagation delay between neighbouring nodes is zero.*

Assumption 4. *If the distance between two border links is less than the carrier sensing range, we regard this scenario as an effective carrier sensing scenario. All links*
485 *share the channel capacity equally in this effective carrier sensing scenario.*

Assumption 5. *If the distance between two border links exceeds the carrier sensing range, we regard this scenario as an ineffective carrier sensing scenario and border effect exists.*

Assumption 6. *Capture effect and packet losses caused by collision are ignored.*

490 **Assumption 7.** *Acknowledgements are obtained instantaneously.*

Assumption 8. *Starvation occurs to a link when the link is within carrier sensing range of two border links. In this research, a starvation link is defined as that the achieved goodput of a link is below $\alpha \times G_{average}$, where $\alpha \in [0.0, 0.2]$ is the starvation factor and $G_{average}$ is the average goodput in E.*

495 Assumptions 1 and 2 simplify an IEEE 802.11 WBN as a single-channel single-radio system with a structured topology and an identical configuration

for all nodes. Assumptions 3, 4, and 5 are the conclusions that have been validated through well-known studies such as [18, 29, 34, 41, 42, 60]. Assumptions 6, 7, and 8 simplify the analysis by neglecting the propagation delay, capture effect and interference caused by collision [29, 61, 62].

Next, we define the goodput formulations for saturated traffic demand in effective carrier sensing scenario and ineffective carrier sensing scenario. Finally, we provide an example illustrating the applications of this model.

4.1.1. Goodput distribution model for saturated traffic demand in effective carrier sensing scenario

Simulation results show that the disk-graph model can predict goodput pattern accurately in effective carrier sensing scenarios with saturated traffic demand (see Section 3.2). Hence, Def. 1 establishes the goodput defined by typical disk-graph models in effective carrier sensing scenarios where all nodes are within each other's carrier sensing range.

Definition 1. *The goodput in effective carrier sensing scenarios with saturated traffic:* Assume that the channel capacity shared among the links in E has normalised as capacity 1 with respect to the maximum net bandwidth. The goodput $G(i)$ of a tagged link i is defined as the ratio between goodput and maximum net bandwidth.

$$G(i) = \frac{1}{N} \quad , \quad \text{when} \quad D \leq R_{cs}, \quad (1)$$

whereby R_{cs} is the carrier sensing range, D is the Cartesian distance between two border links, and N is the number of links in the E .

The proof is given in Appendix A and is immediate by Def. 1 and induction on the number of links in the WBN.

4.1.2. Goodput distribution model for saturated traffic demand in ineffective carrier sensing scenario

For ineffective carrier sensing scenarios that not all nodes are within each other's carrier sensing range, we first discuss the theorem relating goodput

with the notions of independent set and conflict set of a given link i . Based on the theorem 1, we derive of pessimistic and optimistic goodput $G_P(i)$ and $G_O(i)$ for each link i . More details can be found in our previous paper [19].

Theorem 1. *Goodput of a tagged link i in ineffective carrier sensing scenario ($D > R_{CS}$) is a function of $\bar{IS}(i)$ and $\bar{\gamma}(i)$.*

Definition 2. Independent set: *Let E denote the complete set of links in a WBN. For a tagged link i in E , the independent set,*

$$\bar{IS}(i) = \{l \in E \setminus \{i\} \mid d_{s,s} > R_{cs} \text{ and } d_{s,r} > R_{cs}\}. \quad (2)$$

whereby $d_{s,s}$ is the distance between two senders in link l and link i , $d_{s,r}$ is the distance between the sender in link l and the receiver in link i , R_{cs} is the carrier sensing range.

Definition 3. Conflict set: *The conflict set of a tagged link i ,*

$$\bar{\gamma}(i) = \{l \in E \setminus \{i\} \mid d_{s,s} \leq R_{cs} \text{ or } d_{s,s} > R_{cs}, d_{s,r} \leq R_{cs}\}. \quad (3)$$

whereby $d_{s,s}$ is the distance between two senders in link l and link i , $d_{s,r}$ is the distance between the sender in link l and the receiver in link i , R_{cs} is the carrier sensing range and it is clear that $\bar{IS}(i) \cup \bar{\gamma}(i) \cup i = E$.

To derive the goodput model, we define the border-link sets (GCS_{LB} and GCS_{RB}) and middle-link set (GCS_{ML}) based on our previous study [19, 63].

Definition 4. Left and right border-link sets GCS_{LB} and GCS_{RB} :

Let E denote the complete set of links in a WBN. For E , the left border-link set GCS_{LB} and right border-link set GCS_{RB} ,

$$\begin{aligned} GCS_{LB} &= \{l \in E \mid d_{l,RB} > R_{cs}\}, \\ GCS_{RB} &= \{l \in E \mid d_{l,LB} > R_{cs}\}, \end{aligned} \quad (4)$$

whereby $d_{l,LB}$ is the distance between a link l and the left border link, $d_{l,RB}$ is the distance between a link l and the right border link, and R_{cs} is the carrier sensing range.

Definition 5. Middle-link set GCS_{ML} : Let E denote the complete set of links in a WBN. For E , the middle link set GCS_{ML} ,

$$GCS_{ML} = \{l \in E \setminus l \in GCS_{LB} \text{ or } GCS_{RB} \}, \quad (5)$$

545 We further define the dominant left and right border-link sets GCS'_{LB} and GCS'_{RB} as follows:

Definition 6. Dominant Border-link sets GCS'_{LB} and GCS'_{RB}

Let E denote the complete set of links in a WBN. For E , the left dominant border-link set GCS'_{LB} and right dominant border-link set GCS'_{RB} ,

$$\begin{aligned} GCS'_{LB} &= \{l \in GCS_{LB} \mid d_{l,i} > R_{cs} \{i \in GCS'_{RB}\} \}, \\ GCS'_{RB} &= \{l \in GCS_{RB} \mid d_{l,i} > R_{cs} \{i \in GCS'_{LB}\} \}, \end{aligned} \quad (6)$$

550 whereby $d_{l,i}$ is the distance between sender nodes in link l and link i , and R_{cs} is the carrier sensing range.

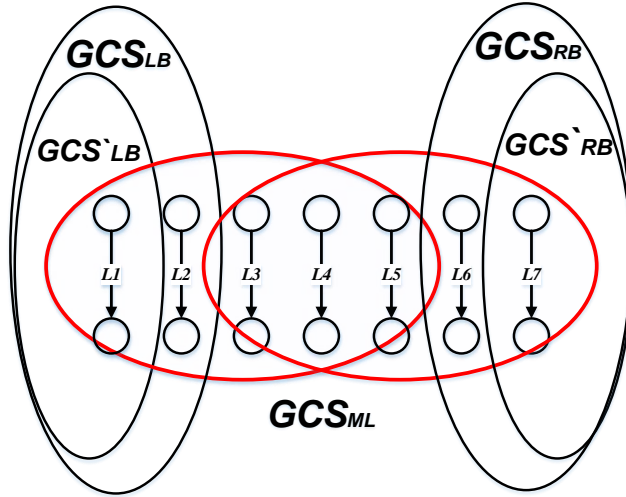


Figure 9: An example of border-link sets, dominant border-link sets, and middle-link set

We use the topology shown in Figure 9 to illustrate the definitions of these border-link sets and middle-link set. Based on the Def. 4, Def. 5, and Def. 6,

we select the border-link sets and a middle-link set in Figure 9. Two red circles
 555 denote the carrier sensing range of left border link $L1$ and right border link $L7$.
 First, we select left border-link set as $GCS_{LB} = \{L1, L2\}$ and right border-link
 set as $GCS_{RB} = \{L6, L7\}$. Middle-link set is $GCS_{ML} = \{L3, L4, L5\}$. Next,
 we remove links $L2$ and $L6$ from the left border-link set GCS_{LB} and GCS_{RB}
 respectively because the distance between links $L2$ and $L6$ is less than the carrier
 560 sensing range. Then, we select dominant border-link sets as $GCS'_{LB} = \{L1\}$
 and $GCS'_{RB} = \{L7\}$.

Next, the minimum global conflict clique γ^{GMC} is defined to calculate the
 spatial capacity in an IEEE 802.11 WBN. Different from the effective carrier
 sensing scenario without spatial reuse, spatial reuse exists in an ineffective
 565 carrier sensing scenario. Because the border links are out of each other's
 carrier sensing range and cannot sense each other, these links can transmit at the
 same time using an identical channel. Therefore, from the perspective of the
 whole network, the spatial capacity may exceed 1. The minimum global con-
 flict clique γ^{GMC} is used to estimate the spatial capacity from the global view
 570 of a network.

For a graph E , a minimum global conflict clique is defined as a set of conflict
 sets $\gamma(i)$ that contains all the links in E following the constraint in Def. 7.

Definition 7. *Minimum global conflict clique γ^{GMC} : For a E ,*

$$\gamma^{GMC} : \{i, i \in E, j \in E : IS(i) \cap IS(j) = \emptyset\} \quad (7)$$

whereby $IS(i)$ is the independent set of link i .

575 In the topology in Figure 9, a minimum global conflict clique is $\{L1, L7\}$.
 The conflict sets of links $L1$ and $L7$ are $\gamma(L1) \cup \gamma(L7) = E$ and the correspond-
 ing independent sets are $IS(L1) \cap IS(L7) = \emptyset$. Then in this topology, the max-
 imum spatial capacity will be $|\gamma^{GMC}| = |\{L1, L7\}| = 2$.

The goodput distribution model is proposed with a pessimistic goodput
 580 $G_P(i)$ and an optimistic goodput $G_O(i)$. This idea arises from two distinct situ-
 ations. The first situation is that the conflicting links of a given link are within

each other's R_{cs} (e.g. all conflicting links of $L1$ are within each other's R_{cs} in Figure 4). In this case, the sum of goodput of a tagged link i and all conflicting links will be 1, $G(i) + \sum_{j \in \gamma(i)} G(j) = 1$. Second situation is that the conflicting links of a given link are not all within each other's R_{cs} (e.g. $L2$'s conflict set is $\{1, 3\}$ but $L1$ and $L3$ are out of each other's R_{cs}). Unlike the previous case, sum of goodput of $L2$ and its conflicting links $L1$ and $L3$ cannot exceed their total goodput 1, i.e. $1 < G(i) + \sum_{j \in \gamma(i)} G(j) \leq |\tilde{\gamma}^{GMC}|$.

To address the two distinct situations, we propose the pessimistic and optimistic estimate of the goodput for a given link i . For the pessimistic estimate of goodput for a tagged link, we restrict the upper bound of the achievable goodput such that $G_P(i) + \sum_{j \in \gamma(i)} G_P(j) = 1$. We regard it as the pessimistic goodput estimate.

In terms of the optimistic estimate of the goodput, we use the conflict set of the border link for the links within the conflict set of the border link. It is because the border link attains the highest goodput and has the fewest number of links in its conflict set. Hence, we restrict the upper bound of the achievable goodput such that $G_P(i) + \sum_{j \in \gamma(B)} G_P(j) = 1$. We regard it as the optimistic estimate of the goodput.

Definition 8. Pessimistic goodput for ineffective carrier sensing scenarios with saturated traffic $G_P(i)$: The pessimistic goodput is defined as the ratio between goodput and maximum net bandwidth,

$$G_P(i) = \begin{cases} 0, & i \in GCS_{ML}, \\ \frac{\chi(i)}{\chi(i) + \sum_{j \in \gamma(i)} \chi(j)} \times \left(1 - |GCS_{ML}| \times \alpha \times \frac{|\tilde{\gamma}^{GMC}|}{N} \right), & \text{otherwise,} \end{cases} \quad (8)$$

subject to $G_P(i) + \sum_{j \in \gamma(i)} G_P(j) = 1$, where $\chi(i)$ is the number of links in a given $\bar{I}S(i)$, $\gamma(i)$ is the conflict set of link i , $|GCS_{ML}|$ is the cardinality of the global middle link set GCS_{ML} , $|\tilde{\gamma}^{GMC}|$ is the cardinality of the minimum global clique $\tilde{\gamma}^{GMC}$, N is the number of links in E and α is the starvation factor.

Definition 9. Optimistic goodput for ineffective carrier sensing scenarios with saturated traffic $G_O(i)$: The optimistic goodput is defined as the ratio of goodput and maximum net bandwidth,

$$G_O(i) = \begin{cases} \alpha \times \frac{|\bar{\gamma}^{GMC}|}{N} & , \quad i \in GCS_{ML}, \\ \frac{\chi(i)}{\chi(i) + \sum_{j \in \gamma(\bar{B})} \chi(j)} & , \quad \text{otherwise,} \end{cases} \quad (9)$$

610 subject to $G_O(B) + \sum_{j \in \gamma(\bar{B})} G_O(j) = 1$, where $\gamma(\bar{B})$ is the conflict set of the border link B in which the link i is and $\chi(i)$ is the number of links in a given $\bar{IS}(i)$, $|\bar{\gamma}^{GMC}|$ is the cardinality of the minimum global clique $\bar{\gamma}^{GMC}$, N is the number of links in E and α is the starvation factor.

Proofs of the pessimistic and optimistic goodput are by definition and in-
615 duction on the number of links in the WBN and is given in Appendix B.

4.1.3. Example: using the model with saturated traffic demand

For saturated traffic demand, we demonstrate the utility of our model with an example in a 600×20 m^2 topology shown in Figure 10. In Figure 10, we select a linear, uniformly spaced and symmetric topology that the network size
620 D is 600 m and the inter-link interval d is 100 m. The network E for this scenario is $E = \{L1, L2, \dots, L7\}$. The transmitter-receiver separation of all links is 20 m. The propagation model is the two-ray propagation model and carrier sensing range R_{cs} is 435 m. The traffic demand of each link is configured as 48 Mbps (for saturating the wireless link).

625 We first calculate the independent set $\bar{IS}(i)$ and conflict set $\bar{\gamma}(i)$ of all links based on the topology information and the given R_{cs} (see Table 3). According to the results tabulated in Table 3, links $L3$ to $L5$ are within the R_{cs} of both border links $L1$ and $L7$ and these middle links have no independent links as $\{\emptyset\}$. We predict that links 3 to 5 will achieve “zero” goodput for pessimistic goodput (and hence are called starving links). We calculate $\bar{\gamma}^{GMC} = \{L1, L7\}$
630 and $|\bar{\gamma}^{GMC}| = 2$. For the optimistic goodput of starving links (assume $\alpha = 0.2$),

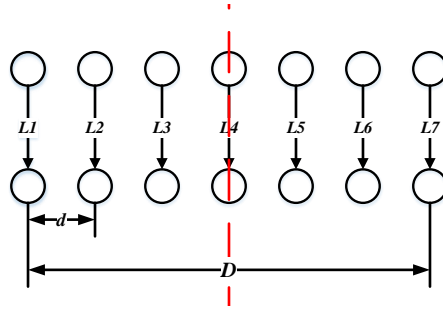


Figure 10: 7 Links deployed in a $d = 100 m$, $600 \times 20 m^2$ WBN

Table 3: Independent sets, conflict sets, and goodput of individual links

Link i	$\bar{I}S(i)$	$\bar{\gamma}(i)$	$\chi(i)$	$G_P(i)$	$G_O(i)$
1	{6,7}	{2,3,4,5}	2	0.610	0.667
2	{7}	{1,3,4,5,6}	1	0.229	0.333
3	$\{\emptyset\}$	{1,2,4,5,6,7,8,9,10}	0	0.0	0.057
4	$\{\emptyset\}$	{1,2,3,5,6,7,8,9,10,11}	0	0.0	0.057
5	$\{\emptyset\}$	{1,2,3,4,6,7,8,9,10,11}	0	0.0	0.057
6	{1}	{2,3,4,5,7}	1	0.229	0.333
7	{1,2}	{3,4,5,6}	2	0.610	0.667

we calculated it as $\alpha \times \frac{|\bar{\gamma}^{GMC}|}{N} = 0.057$.

For the non-starving links, we assign the weight to each link based on definition of $\chi(i)$. For example, link $L2$'s independent set has only one link $L7$, thus we assign link $L2$'s weight as 1, and same for link $L2$ with weight 2. Using Def. 8 and Def. 9, we calculate the pessimistic and optimistic goodput $G_P(i)$ and $G_O(i)$ for this example in Table 3.

4.2. A goodput distribution model for unsaturated traffic demand

In this subsection, we derive the goodput model with unsaturated traffic demand. As we observe in Section 3, whether starvation would happen with unsaturated traffic demands depends on the traffic demands among border links. When unsaturated traffic demands of border links do not exceed chan-

nel capacity, middle links may not get starved. The assumptions for ineffective carrier sensing scenarios with unsaturated traffic demand are the same as those in Section 4.1 except the Assumption 4. **For unsaturated traffic demand, border effect may not exist even if the distance between two border links exceeds the carrier sensing range. The occurrence of the border effect depends on the traffic demand from the border link sets.**

Next, we define the goodput model for effective and ineffective carrier sensing scenarios followed by an example.

4.2.1. Goodput distribution model for unsaturated traffic demand in effective carrier sensing scenario

Simulation results show that the disk-graph model can predict the goodput pattern accurately in effective carrier sensing scenarios with unsaturated traffic demand (see Section 3.3). Hence, Def. 10 establishes the goodput defined by typical disk-graph models in effective carrier sensing scenarios where all nodes are within each other's carrier sensing range.

Definition 10. *Goodput distribution for effective carrier sensing scenarios with unsaturated traffic:*

$$G(i) = \begin{cases} \frac{1}{N} & , \text{when } \sum_{i \in E} f(i) > 1, \\ f(i) & , \text{when } \sum_{i \in E} f(i) \leq 1, \end{cases} \quad (10)$$

whereby N is the number of links in the E , and $f(i)$ denotes the normalized traffic demand of a link i with respect to the maximum net bandwidth.

The proof for the goodput Def. 10 is given in Appendix C.

4.2.2. Goodput distribution model for unsaturated traffic demand in ineffective carrier sensing scenario

We observed that the expected goodput pattern from the disk-graph model is different from simulation results in the ineffective sensing scenario with unsaturated traffic demand in Section 3. Complex interactions between border

links and middle links exists in ineffective carrier sensing scenario. Therefore, we need to refine this scenarios with a new criterion.

670 For ineffective carrier sensing scenario, we define two criteria, A and B to refine the possible combinations of unsaturated traffic demands. First, criterion A is the sum of traffic demands of the links in the dominant border-link sets GCS'_{LB} and GCS'_{RB} , and this is expressed as: $\sum_{j \in GCS'_{LB} \cap GCS'_{RB}} f(j) \geq 1$. The criterion A is to evaluate whether border effect occurs. If the criterion A holds, 675 the border links will occupy the channel and middle links will have very little chance to transmit packets that leads to flow starvation. If not, border effect and flow starvation will not exist. Criterion B is the sum of traffic demands of the links in the left or right border links with the links in its conflict set $\gamma(\bar{B})$, and this is expressed as: $\sum_{j \in B \cap \gamma(\bar{B})} f(j) \geq 1$. The criterion B is to evaluate 680 whether the channel capacity is sufficient for the border link and the links in its conflict set. If the criterion B holds, the border link will have the priority to occupy the channel than its conflicting links. If not, the border link and its conflicting links will share the channel capacity fairly.

We list four possible combinations of unsaturated traffic demands with two 685 criteria A and B in Table 4. For each condition, we define different equations to calculate goodput distribution. For example, if the traffic demands among all links satisfy condition #2, we will calculate the goodput distribution with Def. 11 and Def. 12.

Table 4: Four unsaturated traffic demands in ineffective carrier sensing scenarios

Condition	Criterion A	Criterion B	Predicted goodput
Condition #1	True	True	Def. 11 and Def. 12
Condition #2	True	False	Def. 11 and Def. 12
Condition #3	False	True	Def. 13 and Def. 14
Condition #4	False	False	Def. 15

Definition 11. *Pessimistic goodput for conditions #1 and #2* $G_p(i)$: The pessimistic goodput of a tagged link i is defined as the ratio between goodput and maxi- 690

imum net bandwidth.

$$G_P(i) = \begin{cases} 0 & , i \in GCS_{ML}, \\ \min(f(i), \frac{\chi(i) \times (1 - \alpha \times |GCS_{ML}| \times \frac{|\bar{\gamma}^{GMC}|}{N})}{\chi(i) + \sum_{j \in \gamma(i)} \chi(j)}) & , \text{ otherwise,} \end{cases} \quad (11)$$

whereby $|GCS_{ML}|$ is the cardinality of the middle-link set GCS_{ML} , $f(i)$ is the normalised traffic demand of a link i with respect to the maximum net bandwidth, $\chi(i)$ denotes the number of links in a given $\bar{IS}(i)$ and $\gamma(i)$ is the conflict set of a tagged link i , $|\bar{\gamma}^{GMC}|$ is the cardinality of the minimum global clique $\bar{\gamma}^{GMC}$, α is the starvation factor and N is the number of links in E .

Definition 12. Optimistic goodput for conditions #1 and #2 $G_O(i)$: The optimistic goodput of a tagged link i is defined as the ratio between goodput and maximum net bandwidth.

$$G_O(i) = \begin{cases} \alpha \times \frac{|\bar{\gamma}^{GMC}|}{N} & , i \in GCS_{ML}, \\ \min(f(i), \frac{\chi(i)}{\chi(i) + \sum_{j \in \gamma(B)} \chi(j)}) & , \text{ otherwise,} \end{cases} \quad (12)$$

whereby GCS_{ML} is middle-link set, $\chi(i)$ denotes the number of links in a given $\bar{IS}(i)$ and $\gamma(B)$ is the conflict set of the border link LB or RB. $f(i)$ denotes the normalized traffic demand of a link i with respect to the maximum net bandwidth, $|\bar{\gamma}^{GMC}|$ is the cardinality of the minimum global clique $\bar{\gamma}^{GMC}$, α is the starvation factor and N is the number of links in E .

Definition 13. Pessimistic goodput for condition #3 $G_P(i)$: The pessimistic goodput of a tagged link i is defined as the ratio between goodput and maximum net bandwidth.

$$G_P(i) = \begin{cases} 0.9 \times \min(f(i), \frac{1 - \sum_{j \in \gamma(B)} f(j)}{|GSB_{ML}|}) & , i \in GCS_{ML}, \\ 0.9 \times f(i) & , i \in GCS'_{LB} \text{ or } GCS'_{RB}, \\ 0.9 \times \min(f(i), \frac{\chi(i) \times (1 - \sum_{j \in GCS'_B} f(j))}{\chi(i) + \sum_{l \in \gamma(i) \text{ and } l \notin GCS'_B} \chi(j)}) & , \text{ otherwise,} \end{cases} \quad (13)$$

whereby GCS'_{LB} and GCS'_{RB} are border-link sets, $\chi(i)$ denotes the number of links in a given $\bar{IS}(i)$ and $\gamma(i)$ is the conflict set of a link i , $|GSB_{ML}|$ is the cardinality of

710 the set GCS_{ML} , and $f(i)$ denotes the normalized traffic demand of a link i with respect to the maximum net bandwidth.

Definition 14. Optimistic goodput for condition #3 $G_O(i)$: The optimistic goodput of a tagged link i is defined as the ratio between goodput and maximum net bandwidth.

$$G_O(i) = \begin{cases} \min(f(i), \frac{1 - \sum_{j \in \gamma(\bar{B})} G_P(j)}{|GSB_{ML}|}) & , i \in GCS_{ML}, \\ f(i) & , i \in GCS'_{LB} \text{ or } GCS'_{RB}, \\ \min(f(i), \frac{\chi(i) \times (1 - \sum_{j \in GCS'_B} f(j))}{\chi(i) + \sum_{l \in \gamma(\bar{i}) \text{ and } l \notin GCS'_B} \chi(j)}) & , \text{otherwise,} \end{cases} \quad (14)$$

715 whereby GCS_{ML} is global middle-link set, $|GSB_{ML}|$ is the cardinality of the set GCS_{ML} , $\chi(i)$ is the number of links in $\bar{S}(i)$, $f(i)$ denotes the normalized traffic demand of a link i with respect to the maximum net bandwidth, and $\gamma(\bar{B})$ is the conflict set of the left or right border link.

Definition 15. Pessimistic and optimistic goodput for condition #4 : The goodput of a tagged link i is defined as the ratio between goodput and maximum net bandwidth.

$$G_P(i) = G_O(i) = f(i), \quad (15)$$

whereby $f(i)$ denotes the normalized traffic demand of a link i with respect to the maximum net bandwidth.

4.2.3. Example: using the model with unsaturated traffic demand

725 Here, we use an example to explain how to calculate goodput distribution with unsaturated traffic demand with the topology in Figure 10. In Table 5, two traffic demands $f(i)$ for all links are selected as 0.8 and 0.1 (normalized traffic demand). For $f(i) = 0.8$, the traffic demands of all links satisfy the condition #1 in Table 4. Hence, we select Def. 11 and Def. 12 to calculate $G_P(i)$ and $G_O(i)$ where α is assumed as 0.2. For $f(i) = 0.1$, the traffic demands of all links satisfy 730 the condition #4 in Table 4. We select Def. 15 to calculate $G_P(i)$ and $G_O(i)$.

Table 5: Goodput estimation of individual links in the topology in Figure 10

Link i	$f(i)$	$G_P(i)$	$G_O(i)$	$f(i)$	$G_P(i)$	$G_O(i)$
1	0.8	0.610	0.667	0.1	0.100	0.100
2	0.8	0.229	0.333	0.1	0.100	0.100
3	0.8	0.000	0.057	0.1	0.100	0.100
4	0.8	0.000	0.057	0.1	0.100	0.100
5	0.8	0.000	0.057	0.1	0.100	0.100
6	0.8	0.229	0.333	0.1	0.100	0.100
7	0.8	0.610	0.667	0.1	0.100	0.100

4.3. Summary

In this section, we derive a goodput distribution model based on the observation of two-link and three-link scenarios in Section 3. This unified goodput model can provide link-level goodput distribution with the given inputs: (i) topology, (ii) carrier sensing range, (iii) traffic demand. In subsequent sections, we validate our goodput model through simulations using different propagation models. **Based on the traffic and carrier sensing conditions, the decision tree of our model is shown in Figure 11.**

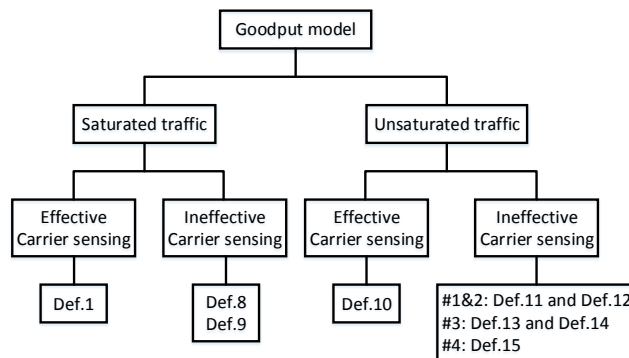


Figure 11: The decision tree of the goodput model

740 5. Simulation validation with two-ray propagation model

In this section, we validate the accuracy of our analytical goodput model through simulation with the two-ray ground model [64]. Two-ray ground model is a typical propagation model in urban environments that are the line-of-sight (LOS) scenarios. According to the two-ray ground model, the received signal includes the signal transmitted through free space and the transmitted signal reflected off the ground. Such two-ray ground model characterises the variation in received signal power due to path loss over distance.

The configuration parameters are listed in Table 1. Similar to the preliminary investigation of disk-graph models in Section 3: (i) we configure all nodes with identical parameters and choose constant bit rate (CBR) unicast transmission as the application with saturated and unsaturated traffic demands (see Table 1); (ii) all nodes are configured with one radio interface and the same channel. Node placement is based on a grid topology (see Figure 12); (iii) we choose transmitter-receiver separation as 20 m to guarantee collision-free transmissions (based on the findings from [65]). Carrier sensing range R_{CS} is calculated as 435 m with the configuration in Table 1.

The topologies we choose will cover effective and ineffective carrier sensing scenarios ranging from $200 \times 20 m^2$ to $800 \times 20 m^2$ (see Figure 12). When the border distance D is less than the carrier sensing range, we regard the scenario as an effective carrier sensing scenario, while when the border distance D is greater than the carrier sensing range, we call that the ineffective carrier sensing scenario.

To validate the accuracy of our analytical model, the goodput model will be used to predict goodput distribution and compared with the simulation mean value. If the mean value of simulation result falls between the prediction of the proposed model, the goodput model predicts the goodput accurately. If not, the error ratio ER is calculated as follows.

Definition 16. *Error Ratio ER*

Let E denote the set of links in an IEEE 802.11 WBN,

$$ER = \left| \frac{(G_s(i) - G_{Mclose}(i))}{G_s} \right|, \quad (16)$$

770 where $G_s(i)$ is the mean goodput of a link i from simulation, $G_{Mclose}(i)$ is the closest goodput prediction from the goodput model.

The results shown for the average goodput in this section are calculated from 100 randomly seeded simulation runs. All averages shown are reported with confidence interval of 95% given by the range of $[0.9to9.8]$ kbps under the
 775 assumption that the averages are normally distributed.

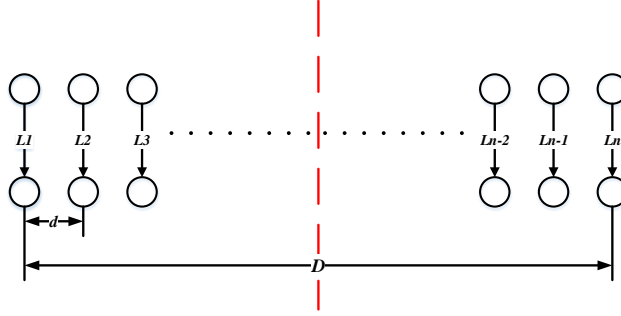


Figure 12: The topology used in the validation

Next, we categorise the simulation results by using two-ray propagation modelare into two parts, saturated and unsaturated traffic demands.

5.1. Saturated Traffic Demand

For saturated traffic demand, the sender of each link in the simulation at-
 780 tempts to transmit packets at the maximal data rate 48 Mbps. Due to space, we list two simulation results for effective and ineffective carrier sensing scenarios. For the effective carrier sensing scenario, we select the topology in Figure 12 with the border distance D as 200 m and $d = 50 m$, where all nodes are within each other's R_{CS} . This example is selected based on the wind turbines con-
 785 nected to the smart grid in Brooklyn, Wellington, New Zealand. Each wind

turbine is installed with a wireless router to exchange data, such as generated energy and error logs (see Figure 13). The inter-link interval in Figure 13 is not identical but we ignore the difference to match with the linear topology in Figure 12.



Figure 13: An example of the effective CSMA scenario in a smart grid system

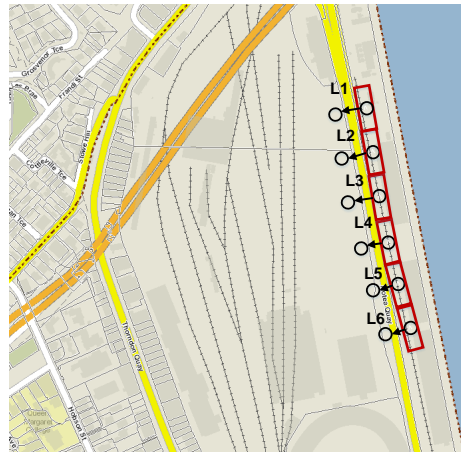


Figure 14: An example of the ineffective CSMA scenario in an intelligent transportation system

790 For ineffective carrier sensing scenarios, we select the topology in Figure 12 with the border distance D as 600 m and $d = 120$ m, where two border links are out of each other's carrier sensing range. We select this example to model the intelligent transportation system (ITS) along the rail track between Wellington and Petone in New Zealand (see Figure 14). The ITS collects data on train load

795 and train delays, and feeds it into a data portal for storage and analysis.

In Tables 6 to 7, the first column refers to the link index in the topology (see Figure 12). Goodput $G_S(i)$ refers to the simulation mean value of goodput. Pessimistic goodput $G_P(i)$ and optimistic goodput $G_O(i)$ are the predictions from our model. ER denotes the difference between $G_S(i)$ and the closest goodput
800 prediction from our model.

Table 6: Goodput of five links in a 200×20 m^2 topology with two-ray propagation model

Link i	$G_S(i)$	$G_P(i)/G_O(i)$	ER
1	0.161	0.200	-
2	0.213*	0.200	0.061
3	0.248*	0.200	0.194
4	0.216*	0.200	0.074
5	0.162	0.200	-

In effective carrier sensing scenario with saturated traffic demand, the results in Table 6 show that different links achieve different goodput. We mark the simulation results that slightly exceed our prediction with (*). In our model, we assume that all links share the channel capacity, which matches with the ex-
805 pectation from disk-graph model. However, in practice there is a small variation in goodput among all the links. We notice that middle links achieve higher goodput than the border links. It implies that even in effective carrier sensing scenarios, the back-off scheme cannot control the media access fairly. We have noticed and explained this problem in Section 3.2. The overall different ratio is
810 below 20%.

For the ineffective scenario, we choose the topology with a fixed border distance, $D = 600$ m to ensure that the two border links are always out of each other's R_{cs} and border effect should occur. Table 7 display the comparison between the results from simulations and those from our analytical model. The
815 gray cells in these two tables denote the links we identified as starving links.

The data in Table 7 shows our model predicts starving links correctly. For

Table 7: Goodput of six links in a $600 \times 20 m^2$ topology with two-ray propagation model

Link i	$G_S(i)$	$G_P(i)$	$G_O(i)$	ER
1	0.614	0.552	0.667	-
2	0.328	0.250	0.333	-
3	0.034	0.000	0.067	-
4	0.034	0.000	0.067	-
5	0.328	0.250	0.333	-
6	0.616	0.552	0.667	-

the non-starving links, all the simulation mean values fall between the range of the predictions from our model. In ineffective carrier sensing scenarios with saturated traffic demands, our model provides accurate prediction of starvation and goodput.

5.2. Unsaturated traffic demand

To validate our model with unsaturated traffic demand, we select three unsaturated traffic demands by using different inter-packet intervals. The traffic demands $f(i)$ at the application layer can be normalized as 0.8, 0.6, 0.4, and 0.1 with the above inter-packet intervals and the configuration parameters in Table 1. As same as the above subsection, we select the same two topologies that represent effective and ineffective carrier sensing scenarios.

Table 8: Goodput of five links in a $200 \times 20 m^2$ topology with two-ray propagation model

Link i	$f(i)$	$G_S(i)$	$G_P(i)/G_O(i)$	ER	$f(i)$	$G_S(i)$	$G_P(i)/G_O(i)$	ER
1	0.8	0.161	0.200	-	0.6	0.161	0.200	-
2	0.8	0.214*	0.200	0.065	0.6	0.214*	0.200	0.065
3	0.8	0.249*	0.200	0.197	0.6	0.251*	0.200	0.203
4	0.8	0.214*	0.200	0.065	0.6	0.214*	0.200	0.065
5	0.8	0.162	0.200	-	0.6	0.161	0.200	-

Table 9: Goodput of five links in a 200×20 m^2 topology with two-ray propagation model—continued

Link i	$f(i)$	$G_S(i)$	$G_P(i)/G_O(i)$	ER	$f(i)$	$G_S(i)$	$G_P(i)/G_O(i)$	ER
1	0.4	0.162	0.200	-	0.1	0.100	0.100	-
2	0.4	0.214*	0.200	0.065	0.1	0.100	0.100	-
3	0.4	0.253*	0.200	0.209	0.1	0.100	0.100	-
4	0.4	0.212*	0.200	0.057	0.1	0.100	0.100	-
5	0.4	0.160	0.200	-	0.1	0.100	0.100	-

For the effective carrier sensing scenario ($D = 200$ m), we list the results in Tables 8 and 9. The function $f(i)$ refers to the traffic demand while goodput $G_S(i)$ and $G_P(i)/G_O(i)$ denote the simulation goodput mean values and the predicted goodput from our model.

The results show the same goodput pattern as that in saturated traffic demand. Only in the case $f(i) = 0.1$, all links achieve the same goodput. For other traffic demands, there is a small variation in goodput among all the links. Along the same lines of explanation in Section 5.1, in effective carrier sensing scenarios, the randomised binary exponential back-off scheme used in IEEE 802.11 carrier sensing may result in a slight difference among the goodput of neighbouring links rather than achieving extreme equal goodput for each link [66]. The overall error is below 21%.

Tables 10 and 11 list the results with unsaturated traffic demands in the ineffective carrier sensing scenarios where D is selected as 600 m and d as 120 m. Results in Tables 10 and 11 show that most of the simulation mean values fall between our prediction range, proving our model predicts starvation and goodput distribution accurately. When $f(i) = 0.6$, in links 2 and 5, we notice a small difference between the simulation results and our prediction. The overall error is below 2%.

Table 10: Goodput of six links in a $600 \times 20 m^2$ topology with two-ray propagation model

Link i	$f(i) = 0.8$				$f(i) = 0.6$			
	$G_S(i)$	$G_O(i)$	$G_P(i)$	ER	$G_S(i)$	$G_O(i)$	$G_P(i)$	ER
1	0.641	0.552	0.667	-	0.600	0.486	0.600	-
2	0.328	0.250	0.333	-	0.339*	0.250	0.333	0.018
3	0.016	0.000	0.067	-	0.026	0.000	0.067	-
4	0.016	0.000	0.067	-	0.027	0.000	0.067	-
5	0.327	0.250	0.333	-	0.339*	0.250	0.333	0.018
6	0.641	0.552	0.667	-	0.600	0.486	0.600	-

Table 11: Goodput of six links in a $600 \times 20 m^2$ topology with two-ray propagation model-continued

Link i	$f(i) = 0.4$				$f(i) = 0.1$			
	$G_S(i)$	$G_P(i)$	$G_O(i)$	ER	$G_S(i)$	$G_P(i)$	$G_O(i)$	ER
1	0.400	0.360	0.400	-	0.1	0.100	0.100	-
2	0.356	0.300	0.400	-	0.1	0.100	0.100	-
3	0.0939	0.090	0.170	-	0.1	0.100	0.100	-
4	0.0932	0.090	0.170	-	0.1	0.100	0.100	-
5	0.355	0.300	0.400	-	0.1	0.100	0.100	-
6	0.400	0.360	0.400	-	0.1	0.100	0.100	-

6. Simulation validation with two-ray shadowing propagation model

In this section, we use the two-ray shadowing propagation model [64] in our simulations to demonstrate the generalizability of our model. Two-ray shadowing model can be superimposed to represent the path loss over distance with the random attenuation from shadowing. Shadowing is generally caused by obstacles between the sender and receiver. These obstacles absorb, reflect, scatter, and diffract the transmitted signal that cause attenuation. The variation of signal due to shadowing is proportional to the length of the obstacles. Similar to the two-ray ground model, the two-ray shadowing model characterises the variation in received signal power due to path loss and shadowing over

distance.

We select two application scenarios in the indoor built environments. For the effective carrier sensing scenario, we select the topology in Figure 12 with the border distance D as 200 m and $d = 50$ m, where all nodes are within each other's R_{CS} . The topology is based on the scenario of the WiFi network at a building in the Kelburn campus of Victoria University of Wellington, Wellington, New Zealand in Figure 15. All the routers in Figure 15 are placed within each other's carrier sensing range.

For ineffective carrier sensing scenarios, we select the topology in Figure 12 with the border distance D as 425 m and $d = 85$ m, where two border links are out of each other's carrier sensing range. This topology is selected based on the smart grid in a residential area in Wellington, New Zealand in Figure 16. The whole area exceeds the carrier sensing range.

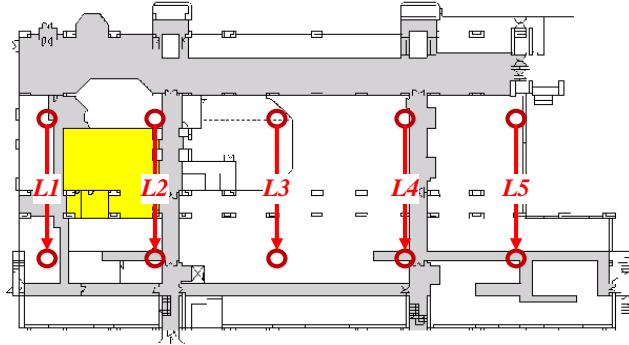


Figure 15: An example of the effective CSMA scenario in a building

For two-ray ground shadowing model, we select three shadowing attenuation δ as 2, 4, and 6. The greater number of shadowing attenuation, the more obstacles exist in the propagation path. The higher the value of shadowing attenuation δ is, the greater the number of obstructions along the propagation path is assumed to be. The carrier sensing range R_{CS} for δ as 2, 4, and 6 is 340 m, 270 m, and 215 m respectively.

The simulation results are presented in two parts: saturated and unsatu-

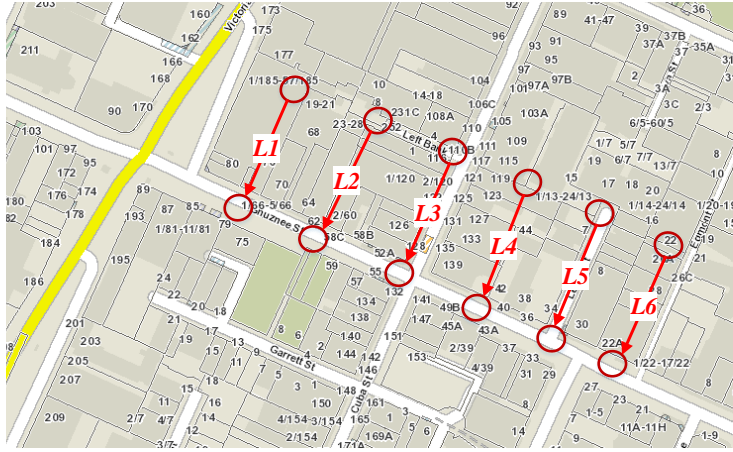


Figure 16: An example of the ineffective CSMA scenario in CBD

rated traffic demands.

6.1. Saturated traffic demand

Table 12: Goodput of five links in a 200×20 m^2 topology with two-ray shadowing propagation model

Link i	Propagation Model $G_p(i)/G_O(i)$	Shadowing ($\delta = 2$)		Shadowing ($\delta = 4$)		Shadowing ($\delta = 6$)	
		$G_S(i)$	ER	$G_S(i)$	ER	$G_S(i)$	ER
1	0.2	0.1570	-	0.156	-	0.166	-
2	0.2	0.223*	0.103	0.226*	0.115	0.219*	0.087
3	0.2	0.238*	0.160	0.236*	0.153	0.230*	0.130
4	0.2	0.226*	0.115	0.224*	0.107	0.219*	0.087
5	0.2	0.156	-	0.116	-	0.166	-

880 For saturated traffic demand, we select three topologies for effective and ineffective carrier sensing scenarios. Table 12 shows the results of effective carrier sensing scenario ($D = 200$ m). We found that adding a shadowing factor in the propagation model does not change the goodput pattern observed in two-ray propagation model. The links in the effective carrier sensing scenario

Table 13: Goodput of six links in a $425 \times 20 \text{ m}^2$ topology with two-ray shadowing propagation model

Link i	Shadowing ($\delta = 2$)				Shadowing ($\delta = 4$)				Shadowing ($\delta = 6$)			
	$G_S(i)$	$G_P(i)$	$G_O(i)$	ER	$G_S(i)$	$G_P(i)$	$G_O(i)$	ER	$G_S(i)$	$G_P(i)$	$G_O(i)$	ER
1	0.616	0.552	0.667	-	0.647	0.552	0.667	-	0.515	0.450	0.500	-
2	0.328	0.250	0.333	-	0.330	0.25	0.333	-	0.314	0.286	0.333	-
3	0.034	0.000	0.067	-	0.012	0.000	0.067	-	0.171*	0.111	0.167	0.023
4	0.034	0.000	0.067	-	0.012	0.000	0.067	-	0.170*	0.111	0.167	0.018
5	0.328	0.250	0.333	-	0.329	0.250	0.333	-	0.314	0.286	0.333	-
6	0.616	0.552	0.667	-	0.648	0.552	0.667	-	0.515	0.450	0.500	-

do not share the channel capacity equally. Middle links achieve higher goodput
885 than the border links. But in Table 12, the overall error is below 16%, which is lower than that in the two-ray propagation model. The same explanation about ineffective back-off scheme has been listed in Section 5.1.

For ineffective scenarios, we choose the fixed border distance, 425 m and d
as 85 m. Tables 13 shows that our model predicts starvation accurately and few
890 errors happen in the scenarios where shadowing attenuation is configured as 6. The overall error is below 2.5%.

6.2. Unsaturated traffic demand

For unsaturated traffic demand, we only list the results by choosing shadowing
attenuation δ as 4 due to space. Shadowing attenuation $\delta = 4$ is the
895 default value in QualNet 5.2 that refers to the common indoor environments with four walls.

Tables 14 to 15 list the results from effective carrier sensing scenario ($D =$
200 m). When the sum of traffic demands of all links exceed the channel capacity, we still can notice the difference of goodput between middle links and
900 border links. The overall error is below 17%. The same explanation about ineffective back-off scheme has been listed in Section 5.1.

For the ineffective carrier sensing scenarios ($D = 425 \text{ m}$ and $d = 85 \text{ m}$), our model can predict starving links correctly in Tables 16 to 17. Few simulation

Table 14: Goodput of five links in a 200×20 m^2 topology with two-ray shadowing propagation model ($\delta = 4$)

Link i	$f(i)$	$G_S(i)$	$G_P(i)/G_O(i)$	ER	$f(i)$	$G_S(i)$	$G_P(i)/G_O(i)$	ER
1	0.8	0.154	0.200	-	0.6	0.156	0.200	-
2	0.8	0.225*	0.200	0.111	0.6	0.224*	0.200	0.107
3	0.8	0.239*	0.200	0.163	0.6	0.237*	0.200	0.156
4	0.8	0.224*	0.200	0.107	0.6	0.228*	0.200	0.123
5	0.8	0.157	0.200	-	0.6	0.156	0.200	-

Table 15: Goodput of five links in a 200×20 m^2 topology with two-ray shadowing propagation model ($\delta = 4$)—continued

Link i	$f(i)$	$G_S(i)$	$G_P(i)/G_O(i)$	ER	$f(i)$	$G_S(i)$	$G_P(i)/G_O(i)$	ER
1	0.4	0.154	0.200	-	0.1	0.100	0.100	-
2	0.4	0.226*	0.200	0.115	0.1	0.100	0.100	-
3	0.4	0.239*	0.200	0.163	0.1	0.100	0.100	-
4	0.4	0.226*	0.200	0.115	0.1	0.100	0.100	-
5	0.4	0.155	0.200	-	0.1	0.100	0.100	-

Table 16: Goodput of six links in a 425×20 m^2 topology with two-ray shadowing propagation model ($\delta = 4$)

Link i	$f(i) = 0.8$				$f(i) = 0.6$			
	$G_S(i)$	$G_O(i)$	$G_P(i)$	ER	$G_S(i)$	$G_O(i)$	$G_P(i)$	ER
1	0.648	0.552	0.667	-	0.600	0.486	0.600	-
2	0.329	0.250	0.333	-	0.344*	0.250	0.333	0.032
3	0.012	0.000	0.067	-	0.023	0.000	0.067	-
4	0.012	0.000	0.067	-	0.023	0.000	0.067	-
5	0.330	0.250	0.333	-	0.344*	0.250	0.333	0.032
6	0.647	0.552	0.667	-	0.600	0.486	0.600	-

905 results of non-starving links are out of the range of our prediction. The overall error is below 7.1%.

Table 17: Goodput of six links in a $425 \times 20 \text{ m}^2$ topology with two-ray shadowing propagation model ($\delta = 4$)-continued

Link i	$f(i) = 0.4$				$f(i) = 0.1$			
	$G_S(i)$	$G_P(i)$	$G_O(i)$	ER	$G_S(i)$	$G_P(i)$	$G_O(i)$	ER
1	0.400	0.360	0.400	-	0.1	0.100	0.100	-
2	0.366	0.300	0.400	-	0.1	0.100	0.100	-
3	0.084*	0.090	0.170	0.071	0.1	0.100	0.100	-
4	0.084*	0.090	0.170	0.071	0.1	0.100	0.100	-
5	0.366	0.300	0.400	-	0.1	0.100	0.100	-
6	0.400	0.360	0.400	-	0.1	0.100	0.100	-

7. Conclusion

To improve IEEE 802.11 WBN planning, a new goodput distribution model is developed with consideration of topology, both effective and ineffective carrier sensing conditions, and saturated and unsaturated traffic demands. The results from simulations show that the new goodput model can predict correctly the dominating border links and the extent of starvations as well with different propagation models and network sizes.

Such a goodput model is useful for network planning in IEEE 802.11 WBNs from different aspects. First, the proposed model is simple and accurate to predict potential performance such as goodput and fairness in an IEEE 802.11 WBN. Moreover, this model can be easily integrated into a network design tool. Second, this model helps guide node placement to prevent flow starvation in the planning stage. Finally, this model is useful for optimising the IEEE 802.11 protocols such as channel assignment and routing with an accurate prediction of link quality.

To further improve the accuracy of our model, we will validate our goodput model through test-bed experiments and refine the model in future.

Appendix A. Goodput for effective carrier sensing with saturated traffic assumption

925 **Proof 1.** Let N denote the number of links in a given WBN and $f(i)$ the normalised traffic demand of a given link i with respect to the maximum net bandwidth.

For $N = 1$, then there is one link L_1 in the WBN. If the traffic demand of this link $f(L_1) = 1$, then L_1 achieves the full capacity:

$$G(L_1) = \frac{1}{N} = 1.$$

930 For $N = 2$, there are two links L_1 and L_2 in the WBN. If the traffic demand of these two links is $f(L_1) = f(L_2) = 1$, the sum of the traffic demands of these two links exceeds the capacity $f(L_1) + f(L_2) > 1$, then these two links have to share the capacity and achieve goodput:

$$G(L_1) = G(L_2) \text{ and } G(L_1) + G(L_2) = 1.$$

935 Therefore, $G(L_i) = \frac{1}{N}$, $\forall i \in N$.

For $N = k$, there are k links L_1, \dots and L_k in the WBN. If the traffic demand of these k links is $f(L_1) = \dots = f(L_k) = 1$, the sum of the traffic demands of these k links exceeds the capacity $\sum_{j \in k} f(j) > 1$, then these k links have to share the capacity and achieve:

940 $G(L_1) = G(L_1) \dots = G(L_k) \text{ and } \sum_{j \in k} f(j) > 1.$

Therefore, we have $G(L_i) = \frac{1}{N}$, $\forall i \in N$.

By induction on N , the goodput for a given link for saturated traffic demand in effective carrier sensing scenario in Def. 1.

Appendix B. Pessimistic and optimistic goodput under ineffective CSMA with saturated traffic assumption

945

Proof 2. Let N be the number of links in a given WBN, $f(i)$ is the normalised traffic demand of a given link i with respect to the maximum net bandwidth, $\bar{I}S(i)$ and $\bar{\gamma}(i)$ are the independent set and conflict set of a given link i .

Let $N = 3$, there are three links $L_1, L_2,$ and L_3 in the WBN (see Figure B.17). By

950 Def. 3, the conflict set of each link $i, i \in \{1, 2, 3\}$ are:

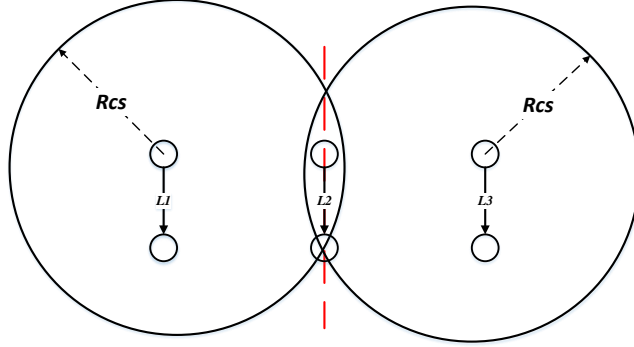


Figure B.17: A three-link WBN

$\bar{\gamma}(L_1) = \{L_2\}$, $\bar{\gamma}(L_2) = \{L_1, L_3\}$, $\bar{\gamma}(L_3) = \{L_2\}$, and by Def. 2 the independent set of each link i is:

$$\bar{I}S(L_1) = \{L_3\}, \bar{I}S(L_3) = \{L_1\}, \bar{I}S(L_2) = \{\emptyset\}.$$

Let the traffic demand of each link $f(i) = 1$. As link L_2 is conflict with links L_1 and L_3 , we calculate the pessimistic goodput of link L_2 with the optimistic goodput of links L_1 and L_3 . Because L_2 has no link in its independent set the goodput is zero i.e. $G_P(L_2) = 0.0$, it follows that links L_1 and L_3 will occupy full capacity:

$$G_O(L_1) = \frac{|\bar{I}S(L_1)|}{|\bar{I}S(L_1)| + |\bar{I}S(L_2)|} ,$$

$$G_O(L_3) = \frac{|\bar{I}S(L_3)|}{|\bar{I}S(L_3)| + |\bar{I}S(L_2)|} ,$$

$$G_O(L_1) + G_P(L_2) = 1 \text{ and } G_O(L_2) + G_P(L_3) = 1.$$

By Def. 7, $\bar{\gamma}^{GMC} = \{L_1, L_3\}$ and $|\bar{\gamma}^{GMC}| = 2$. By Def. 9, the optimistic goodput of starving link L_2 is:

$$G_O(L_2) = \alpha \times \frac{|\bar{\gamma}^{GMC}|}{N} = 0.133 \text{ where } \alpha \text{ is selected as } 0.2,$$

which implies that starving link achieves a non-zero goodput. Since starving link L_2 may achieve non-zero goodput, links L_1 and L_3 cannot occupy the whole capacity. Thus, the pessimistic goodput of links L_1 and L_3 will be :

$$G_P(L_1) = \frac{|\bar{I}S(L_1)|}{|\bar{I}S(L_1)| + |\bar{I}S(L_2)|} \times (1 - G_O(L_2)),$$

$$G_P(L_3) = \frac{|\bar{IS}(L_3)|}{|\bar{IS}(L_2)| + |\bar{IS}(L_3)|} \times (1 - G_O(L_2)).$$

From the perspective of links L_1 and L_3 , the sum of goodput in their conflict sets follows: $G_O(L_2) + G_P(L_1) = 1$ and $G_O(L_2) + G_P(L_3) = 1$.

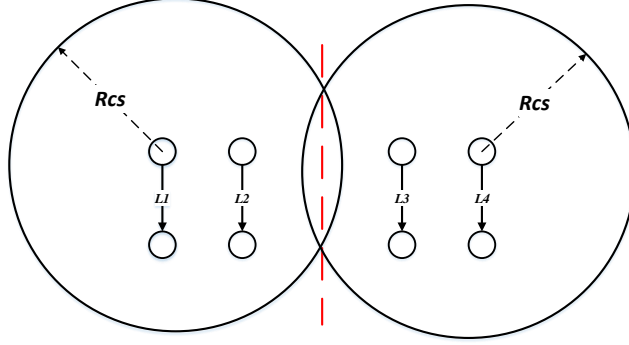


Figure B.18: A four-link WBN

Let $N = 4$, there are four links in Figure B.18. By Def. 3, the conflict set of each link i , $i \in \{1, 2, 3, 4\}$ are:

$$\bar{\gamma}(L_1) = \{L_2\}, \bar{\gamma}(L_2) = \{L_1, L_3\}, \bar{\gamma}(L_3) = \{L_2, L_4\}, \bar{\gamma}(L_4) = \{L_3\}$$

and by Def. 2 the independent set of each link i is:

$$\bar{IS}(L_1) = \{L_3, L_4\}, \bar{IS}(L_2) = \{L_1\}, \bar{IS}(L_3) = \{L_1\}, \bar{IS}(L_4) = \{L_1, L_2\}.$$

Thus, by Eq. (8) no link will be starved because no link is within the carrier sensing range of two border links. It follows that two subgroups $\{L_1, L_2\}$ and $\{L_3, L_4\}$ occupy full capacity for the effective case because two border links are out of each other's carrier sensing range. In each subgroup, the optimistic goodput of a link will be proportional to the number of links in its independent set and the capacity contention is only considered within the conflict set of border link:

$$G_O(L_1) = \frac{|\bar{IS}(L_1)|}{|\bar{IS}(L_1)| + |\bar{IS}(L_2)|},$$

$$G_O(L_2) = \frac{|\bar{IS}(L_2)|}{|\bar{IS}(L_1)| + |\bar{IS}(L_2)|},$$

$$G_O(L_1) + G_O(L_2) = 1.$$

Similarly, the goodput for the other two links are:

$$G_O(L_3) = \frac{|\bar{I}S(L_3)|}{|\bar{I}S(L_3)| + |\bar{I}S(L_4)|} ,$$

$$G_O(L_4) = \frac{|\bar{I}S(L_4)|}{|\bar{I}S(L_3)| + |\bar{I}S(L_4)|} ,$$

$$G_O(L_3) + G_O(L_4) = 1.$$

By Def. 7, $\bar{\gamma}^{\text{GMC}} = \{L_1, L_4\}$ and $\bar{\gamma}^{\text{GMC}} = 2$. Since in this four-link WBN, there
 970 is no starving link. So the pessimistic goodput of links are the same as their optimistic
 goodput following the same assumption that goodput is proportional to the number of
 links in the independent set.

For left border link L_1 , the pessimistic goodput follows $G_P(L_1) + G_P(L_2) = 1$ and is:

$$G_P(L_1) = \frac{|\bar{I}S(L_1)|}{|\bar{I}S(L_1)| + |\bar{I}S(L_2)|} ,$$

975 For link L_2 , $\bar{\gamma}(L_2) = \{L_1, L_3\}$. The pessimistic goodput follows $G_P(L_1) + G_P(L_2) +$
 $G_P(L_3) = 1$ and is:

$$G_P(L_2) = \frac{|\bar{I}S(L_2)|}{|\bar{I}S(L_1)| + |\bar{I}S(L_2)| + |\bar{I}S(L_3)|} .$$

Similarly, the pessimistic goodput of links L_3 and L_4 are:

$$G_P(L_3) = \frac{|\bar{I}S(L_3)|}{|\bar{I}S(L_3)| + |\bar{I}S(L_2)| + |\bar{I}S(L_4)|} ,$$

980
$$G_P(L_4) = \frac{|\bar{I}S(L_4)|}{|\bar{I}S(L_3)| + |\bar{I}S(L_4)|} .$$

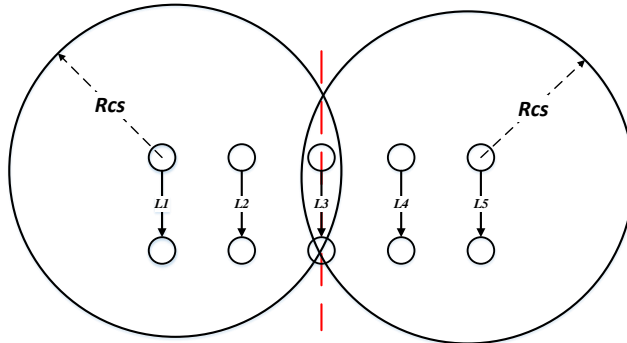


Figure B.19: A five-link WBN

Let $N = 5$, there are five links in Figure B.19. By Def. 3, the conflict set of each link i , $i \in \{1, 2, 3, 4, 5\}$ are:

$$\bar{\gamma}(L_1) = \{L_2, L_3\}, \bar{\gamma}(L_2) = \{L_1, L_3, L_4\}, \bar{\gamma}(L_3) = \{L_1, L_3, L_4, L_5\}, \bar{\gamma}(L_4) = \{L_2, L_3, L_5\}, \bar{\gamma}(L_5) = \{L_3, L_4\}.$$

985 and by Def. 2 the independent set of each link i is:

$$\bar{IS}(L_1) = \{L_4, L_5\}, \bar{IS}(L_2) = \{L_5\}, \bar{IS}(L_3) = \{\emptyset\}, \bar{IS}(L_4) = \{L_1\}, \bar{IS}(L_5) = \{L_1, L_2\}.$$

Assuming $f(i) = 1$, by Eq (8) link L_3 will be starved because L_2 has no link in its independent set i.e. $G_P(L_3) = 0.0$, It follows that two subgroup $\{L_1, L_2\}$ and
 990 $\{L_3, L_4\}$ occupy full capacity for the effective case because two border links are out of each other's carrier sensing range. In each subgroup, the optimistic goodput of a link will be proportional to the number of links in its independent set, and the corresponding expressions for goodput are:

$$G_O(L_1) = \frac{|\bar{IS}(L_1)|}{|\bar{IS}(L_1)| + |\bar{IS}(L_2)| + |\bar{IS}(L_3)|} ,$$

$$G_O(L_2) = \frac{|\bar{IS}(L_2)|}{|\bar{IS}(L_1)| + |\bar{IS}(L_2)| + |\bar{IS}(L_3)|} ,$$

$$G_O(L_1) + G_O(L_2) + G_P(L_3) = 1 .$$

Similarly, for the remaining subgroup:

$$G_O(L_4) = \frac{|\bar{IS}(L_4)|}{|\bar{IS}(L_3)| + |\bar{IS}(L_4)| + |\bar{IS}(L_5)|} ,$$

$$G_O(L_5) = \frac{|\bar{IS}(L_4)|}{|\bar{IS}(L_3)| + |\bar{IS}(L_4)| + |\bar{IS}(L_5)|} ,$$

$$G_O(L_4) + G_O(L_5) + G_P(L_3) = 1 .$$

995 and this yields the solution we call the optimistic goodput.

By Def. 7, $\bar{\gamma}^{GMC} = \{L_1, L_5\}$ and $|\bar{\gamma}^{GMC}| = 2$. By Def. 9, the optimistic goodput of starving link L_3 is:

$$G_O(L_3) = \alpha \times \frac{|\bar{\gamma}^{\text{GMC}}|}{N} = 0.08 \text{ where } \alpha \text{ is selected as } 0.2.$$

Since the starving link achieves non-zero goodput, the pessimistic goodput of other
 1000 links need to consider it. For left border link L_1 , its pessimistic goodput follows
 $G_P(L_1) + G_P(L_2) + G_P(L_3) = 1$ and is:

$$G_P(L_1) = \frac{|\bar{I}S(L_1)|}{|\bar{I}S(L_1)| + |\bar{I}S(L_2)| + |\bar{I}S(L_3)|} \times (1 - G_O(L_3)).$$

For link L_2 , $\bar{\gamma}(L_2) = \{L_1, L_3, L_4\}$. We need to calculate the pessimistic goodput of
 link L_2 with consideration of the effect of link L_4 . $G_P(L_1) + G_P(L_2) + G_P(L_3) +$
 $G_P(L_4) = 1$.

$$G_P(L_2) = \frac{|\bar{I}S(L_1)|}{|\bar{I}S(L_1)| + |\bar{I}S(L_2)| + |\bar{I}S(L_3)| + |\bar{I}S(L_4)|} \times (1 - G_O(L_3)) .$$

1005 With the same reasoning, the pessimistic goodput of links L_4 and L_5 are:

$$G_P(L_5) = \frac{|\bar{I}S(L_5)|}{|\bar{I}S(L_5)| + |\bar{I}S(L_4)| + |\bar{I}S(L_3)|} \times (1 - G_O(L_3)) .$$

For link L_4 , $\bar{\gamma}(L_5) = \{L_2, L_3, L_5\}$. We need to calculate the pessimistic goodput of
 link L_2 with consideration of the effect of link L_4 .

$$G_P(L_4) = \frac{|\bar{I}S(L_4)|}{|\bar{I}S(L_5)| + |\bar{I}S(L_4)| + |\bar{I}S(L_3)| + |\bar{I}S(L_2)|} \times (1 - G_O(L_3)) .$$

By induction on N , we define the pessimistic and optimistic estimate of the goodput
 $G_P(i)$ and $G_O(i)$ for a given link for saturated traffic demand in ineffective carrier
 1010 sensing scenario in Def. 8 and Def. 9.

Appendix C. Goodput for effective carrier sensing with unsaturated traffic assumption

Proof 3. Let N be the number of links in a given WBN and $f(i)$ the normalised traffic demand of a given link i with respect to the maximum net bandwidth.

1015 For $N = 1$, then there is one link L_1 in the WBN. Since the traffic demand of this link $f(L_1) \leq 1$, then L_1 achieves the desired goodput:

$$G(L_1) = f(i).$$

For $N = 2$, there are two links L_1 and L_2 in the WBN. If the sum of the traffic demands of these two links exceeds the capacity $f(L_1) + f(L_2) > 1$, then these two links have
1020 to share the capacity and achieve the goodput as :

$$G(L_1) = G(L_2) = \frac{1}{N} = 0.5.$$

If the sum of the traffic demands of these two links does not exceed the capacity $f(L_1) + f(L_2) \leq 1$, then these two links achieve the desired goodput:

$$G(L_1) = G(L_2) = f(i) \text{ and } G(L_1) + G(L_2) \leq 1.$$

1025 Therefore, $G(L_i) = f(i)$, $\forall i \in N$.

For $N = k$, there are k links L_1, \dots and L_k in the WBN. If the sum of the traffic demands of these k links exceeds the capacity $\sum_{j \in E} f(j) = k > 1$, then these k links have to share the capacity and achieve the goodput as:

$$G(L_1) = \dots = G(L_k) = \frac{1}{k} = \frac{1}{N} \text{ and } G(L_1) + \dots + G(L_k) = 1.$$

1030 Therefore, $G(L_i) = \frac{1}{N}$, $\forall i \in N$.

If the sum of the traffic demands of these k links does not exceed the capacity $\sum_{j \in E} f(j) = k \leq 1$, then these k links achieve desired goodput as:

$$G(L_1) = \dots = G(L_k) = f(i) \text{ and } G(L_1) + \dots + G(L_k) \leq 1.$$

Therefore, $G(L_i) = f(i)$, $\forall i \in N$.

1035 By induction on N , the goodput for a given link for unsaturated traffic demand in effective carrier sensing scenario in Def. 10.

References

- [1] Edhrp: Energy efficient event driven hybrid routing protocol for densely
1040 deployed wireless sensor networks, Journal of Network and Computer
Applications, Elsevier 58 (2015) 309 – 326.
- [2] M. Coldrey, U. Engström, K. W. Helmersson, M. Hashemi, L. Manholm,

P. Wallentin, *Wireless backhaul in future heterogeneous networks*, Ericsson Review 91.

- 1045 [3] T. Q. Quek, G. de la Roche, İ. Güvenç, M. Kountouris, *Small cell networks: Deployment, PHY techniques, and resource management*, Cambridge University Press, 2013.
- [4] X. Fang, S. Misra, G. Xue, D. Yang, The new and improved power grid: A survey, *IEEE Communications Surveys Tutorials* 14 (4) (2012) 944–980.
- 1050 [5] R. Ma, H. H. Chen, Y. R. Huang, W. Meng, *Smart grid communication: Its challenges and opportunities*, *IEEE Transactions on Smart Grid* 4 (1) (2013) 36–46.
- [6] H. S. Dhillon, G. Caire, *Wireless backhaul networks: Capacity bound, scalability analysis and design guidelines*, *IEEE Transactions on Wireless Communications* 14 (11) (2015) 6043–6056.
- 1055 [7] A. Malik, J. Qadir, B. Ahmad, K.-L. A. Yau, U. Ullah, *QoS in IEEE 802.11-based wireless networks: A contemporary review*, *Journal of Network and Computer Applications*, Elsevier 55 (2015) 24–46.
- [8] C. Hua, R. Zheng, *On link-level starvation in dense 802.11 wireless community networks*, *Computer Networks*, Elsevier 54 (17) (2010) 3159–3172.
- 1060 [9] N. Kumar, M. Kumar, R. Patel, *Capacity and interference aware link scheduling with channel assignment in wireless mesh networks*, *Journal of Network and Computer Applications*, Elsevier 34 (1) (2011) 30–38.
- [10] Y. Peng, Y. Yu, L. Guo, D. Jiang, Q. Gai, *An efficient joint channel assignment and QOS ROUTING PROTOCOL FOR IEEE 802.11 multi-radio multi-*
1065 *channel wireless mesh networks*, *Journal of Network and Computer Applications*, Elsevier 36 (2) (2013) 843–857.
- [11] R. Lopes Gomes, W. Moreira Junior, E. Cerqueira, A. Jorge Abelém, *Using fuzzy link cost and dynamic choice of link quality metrics to achieve QoS*

- and QoE in wireless mesh networks, *Journal of Network and Computer Applications*, Elsevier 34 (2) (2011) 506–516.
- 1070
- [12] M. Durvy, O. Dousse, P. Thiran, Border effects, fairness, and phase transition in large wireless networks, in: *Proceedings of the 27th IEEE Conference on Computer Communications (INFOCOM)*, Phoenix, AZ, USA, 2008, pp. 1274–1282.
- 1075
- [13] A. Barolli, F. Xhafa, M. Takizawa, Optimization problems and resolution methods for node placement in wireless mesh networks, in: *the 14th International Conference on Network-Based Information Systems (NBiS)*, IEEE, Tirana, Albania, 2011, pp. 126–134.
- [14] F. Xhafa, C. Sánchez, A. Barolli, M. Takizawa, Solving mesh router nodes placement problem in wireless mesh networks by tabu search algorithm, *Journal of Computer and System Sciences*, Elsevier 81 (8) (2015) 1417–1428.
- 1080
- [15] M. Faheem, V. C. Gungor, Capacity and spectrum-aware communication framework for wireless sensor network-based smart grid applications, *Computer Standards & Interfaces*, Elsevier 53 (2017) 48–58.
- 1085
- [16] Energy efficient and qos-aware routing protocol for wireless sensor network-based smart grid applications in the context of industry 4.0, *Applied Soft Computing*, Elsevier.
- [17] IEEE STD 802.11-1999, Wireless LAN Medium Access Control (MAC) and Physical Layer (PHY) specification.
- 1090
- [18] Y. Qu, B. Ng, The effect of carrier sensing mechanisms on wireless mesh network goodput, in: *Proceedings of Telecommunication Networks and Applications Conference (ITNAC)*, 2015 International, IEEE, Sydney, Australia, 2015, pp. 106–113.
- 1095
- [19] Y. Qu, B. Ng, W. K. G. Seah, A goodput distribution model for IEEE 802.11 wireless mesh networks, in: *Proceedings of the IEEE 34th In-*

ternational Performance Computing and Communications Conference (IPCCC), Nanjing, China, 2015, pp. 1–8.

- 1100 [20] J. Robinson, E. W. Knightly, A performance study of deployment factors in wireless mesh networks, in: the 26th IEEE International Conference on Computer Communications (INFOCOM), Atlanta, GA, USA, 2007, pp. 2054–2062.
- [21] S. Sakamoto, T. Oda, E. Kulla, F. Xhafa, M. Ikeda, L. Barolli, Evaluation of effects of grid shape in WMN-SA system for solution of node placement problem in WMNs, in: Proceedings of the 12th International Conference on Complex, Intelligent and Software Intensive Systems (CISIS), 2014, pp. 113–119.
- 1105 [22] E. Amaldi, A. Capone, F. Malucelli, Planning UMTS base station location: Optimization models with power control and algorithms, *IEEE Transactions on Wireless Communications* 2 (5) (2003) 939–952.
- 1110 [23] D. Bailey, *Practical radio engineering and telemetry for industry*, Elsevier, 2003.
- [24] A. R. Mishra, *Fundamentals of cellular network planning and optimisation: 2G/2.5 G/3G... evolution to 4G*, Wiley, 2004.
- 1115 [25] R. Olexa, *Implementing 802.11, 802.16, and 802.20 Wireless Networks: Planning, Troubleshooting, and Operations*, Elsevier, 2004.
- [26] J. Bicket, S. Biswas, D. Aguayo, R. Morris, Architecture and evaluation of the MIT ROOFNET mesh network.
- 1120 [27] S. Avallone, G. Di Stasi, Design and implementation of wimesh: A tool for the performance evaluation of multi-radio wireless mesh networks, *Journal of Network and Computer Applications*, Elsevier 63 (2016) 98–109.

- [28] S. Bosio, A. Capone, M. Cesana, Radio planning of wireless local area networks, *IEEE/ACM Transactions on Networking* 15 (6) (2007) 1414–1427.
- 1125 [29] M. Garetto, T. Salonidis, E. W. Knightly, Modeling per-flow throughput and capturing starvation in CSMA multi-hop wireless networks, *IEEE/ACM Transactions on Networking (ToN)* 16 (4) (2008) 864–877.
- [30] T. Vanhatupa, M. Hännikäinen, T. D. Hämäläinen, Performance model for IEEE 802.11 s wireless mesh network deployment design, *Journal of Parallel and Distributed Computing*, Elsevier 68 (3) (2008) 291–305.
- 1130 [31] J. Avonts, C. Blondia, A framework to compare topology algorithms in multi-channel multi-radio wireless mesh networks, *Computer Networks*, Elsevier 98 (2016) 89–108.
- [32] K. Medepalli, F. A. Tobagi, Towards performance modeling of IEEE 802.11 based wireless networks: A unified framework and its applications, in: *Proceedings of the 25th IEEE International Conference on Computer Communications (INFOCOM)*, Barcelona, Spain, 2006, pp. 1–12.
- 1135 [33] X. Wang, K. Kar, Throughput modelling and fairness issues in CSMA/CA based ad-hoc networks, in: *Proceedings of the 24th IEEE Conference on Computer Communications (INFOCOM)*, Vol. 1, Miami, Florida, USA, 2005, pp. 23–34.
- 1140 [34] M. W. Lee, G. Hwang, S. Roy, Performance modeling and analysis of IEEE 802.11 wireless networks with hidden nodes, in: *Proceedings of the 16th ACM International Conference on Modeling, Analysis and Simulation of Wireless and Mobile Systems (MSWiM)*, Barcelona, Spain, 2013, pp. 135–142.
- 1145 [35] P. van de Ven, A. J. Janssen, J. van Leeuwen, Balancing exposed and hidden nodes in linear wireless networks, *IEEE/ACM Transactions on Networking (TON)* 22 (5) (2014) 1429–1443.

- 1150 [36] H. Zhao, E. Garcia-Palacios, S. Wang, J. Wei, D. Ma, Evaluating the impact of network density, hidden nodes and capture effect for throughput guarantee in multi-hop wireless networks, *Ad Hoc Networks*, Elsevier 11 (1) (2013) 54–69.
- [37] Y. Qu, B. Ng, W. Seah, A survey of routing and channel assignment in multi-channel multi-radio WMNs, *Journal of Network and Computer Applications*, Elsevier 65 (C) (2016) 120–130.
1155
- [38] O. Goussevskaia, Y. A. Oswald, R. Wattenhofer, Complexity in geometric SINR, in: *Proceedings of the 8th international symposium on Mobile ad hoc networking and computing (MobiHoc)*, ACM, Montral, Qubec, Canada, 2007, pp. 100–109.
1160
- [39] A. Iyer, C. Rosenberg, A. Karnik, What is the right model for wireless channel interference?, *Wireless Communications, IEEE Transactions on* 8 (5) (2009) 2662–2671.
- [40] A. U. Chaudhry, R. H. Hafez, J. W. Chinneck, On the impact of interference models on channel assignment in multi-radio multi-channel wireless mesh networks, *Ad Hoc Networks* 27 (2015) 68–80.
1165
- [41] G. Bianchi, Performance analysis of the IEEE 802.11 distributed coordination function, *IEEE Journal on Selected Areas in Communications* 18 (3) (2000) 535–547.
- 1170 [42] G. Bianchi, I. Tinnirello, Remarks on IEEE 802.11 DCF performance analysis, *IEEE Communications Letters* 9 (8) (2005) 765–767.
- [43] F. Calì, M. Conti, E. Gregori, Dynamic tuning of the IEEE 802.11 protocol to achieve a theoretical throughput limit, *IEEE/ACM Transactions on Networking (ToN)* 8 (6) (2000) 785–799.
- 1175 [44] E. Felemban, E. Ekici, Single hop IEEE 802.11 DCF analysis revisited: Accurate modeling of channel access delay and throughput for saturated and

unsaturated traffic cases, *IEEE Transactions on Wireless Communications* 10 (10) (2011) 3256–3266.

- 1180 [45] F. Daneshgaran, M. Laddomada, F. Mesiti, M. Mondin, Unsaturated throughput analysis of IEEE 802.11 in presence of non ideal transmission channel and capture effects, *IEEE Transactions on Wireless Communications* 7 (4) (2008) 1276–1286.
- [46] Y. S. Liaw, A. Dadej, A. Jayasuriya, Performance analysis of IEEE 802.11 DCF under limited load, in: *Proceedings of the Asia-Pacific Conference on Communications*, IEEE, Perth, Australia, 2005, pp. 759–763.
1185
- [47] M. Ergen, P. Varaiya, Throughput analysis and admission control for IEEE 802.11a, *Mobile Networks and Applications*, Springer 10 (5) (2005) 705–716.
- [48] S. H. Nguyen, H. L. Vu, L. L. Andrew, Performance analysis of IEEE 802.11 WLANs with saturated and unsaturated sources, *IEEE Transactions on Vehicular Technology* 61 (1) (2012) 333–345.
1190
- [49] I. Tinnirello, G. Bianchi, Y. Xiao, Refinements on IEEE 802.11 distributed coordination function modeling approaches, *IEEE Transactions on Vehicular Technology* 59 (3) (2010) 1055–1067.
- 1195 [50] Y. Gao, D.-M. Chiu, J. Lui, Determining the end-to-end throughput capacity in multi-hop networks: methodology and applications, in: *SIGMETRICS Performance Evaluation Review*, Vol. 34, 2006, pp. 39–50.
- [51] P. C. Ng, S. C. Liew, Throughput analysis of IEEE 802.11 multi-hop ad hoc networks, *IEEE/ACM Transactions on Networking (TON)* 15 (2) (2007) 309–322.
1200
- [52] Z. Zeng, Y. Yang, J. C. Hou, How physical carrier sense affects system throughput in IEEE 802.11 wireless networks, in: *Proceedings of the 27th IEEE Conference on Computer Communications (INFOCOM)*, Phoenix, AZ, USA, 2008.

- 1205 [53] J. Simo Reigadas, A. Martinez-Fernandez, J. Ramos-Lopez, J. Seoane-Pascual, Modeling and optimizing IEEE 802.11 DCF for long-distance links, *IEEE Transactions on Mobile Computing* 9 (6) (2010) 881–896.
- [54] P. Stuedi, G. Alonso, Modeling and computing throughput capacity of wireless multihop networks, *Computer Networks*, Elsevier 52 (1) (2008) 116–129.
- 1210 [55] C. Hua, R. Zheng, Starvation modeling and identification in dense 802.11 wireless community networks, in: *Proceedings of the 27th IEEE Conference on Computer Communications (INFOCOM)*, Phoenix, AZ, USA, 2008.
- 1215 [56] S. Ray, D. Starobinski, J. B. Carruthers, Performance of wireless networks with hidden nodes: a queuing-theoretic analysis, *Computer Communications*, Elsevier 28 (10) (2005) 1179–1192.
- [57] R. R. Boorstyn, A. Kershenbaum, B. Maglaris, V. Sahin, Throughput analysis in multihop CSMA packet radio networks, *IEEE Transactions on Communications* 35 (3) (1987) 267–274.
- 1220 [58] G. Zhou, T. He, S. Krishnamurthy, J. A. Stankovic, Impact of radio irregularity on wireless sensor networks, in: *Proceedings of the 2nd international conference on Mobile systems, applications, and services (MobiSys)*, ACM, Boston, Massachusetts, USA, 2004, pp. 125–138.
- 1225 [59] L. Fu, S. C. Liew, J. Huang, Effective carrier sensing in CSMA networks under cumulative interference, *IEEE Transactions on Mobile Computing* 12 (4) (2013) 748–760.
- [60] V. Gambiroza, B. Sadeghi, E. W. Knightly, End-to-end performance and fairness in multihop wireless backhaul networks, in: *Proceedings of the 10th Annual International Conference on Mobile Computing and Networking*, *MobiCom '04*, ACM, Philadelphia, PA, USA, 2004, pp. 287–301.
- 1230

- 1235 [61] Z. Shi, C. Beard, K. Mitchell, Competition, cooperation, and optimization in multi-hop csma networks, in: Proceedings of the 8th ACM Symposium on Performance Evaluation of Wireless Ad Hoc, Sensor, and Ubiquitous Networks, PE-WASUN '11, ACM, New York, NY, USA, 2011, pp. 117–120.
- [62] X. Wang, K. Kar, Throughput modelling and fairness issues in CSMA/CA based ad-hoc networks, in: Proceedings of the 24th Annual Joint Conference of the IEEE Computer and Communications Societies (INFOCOM), Vol. 1, Miami, FL, USA, 2005, pp. 23–34 vol. 1.
- 1240 [63] Y. Qu, B. Ng, H. Yu, Anti-starvation channel assignment with global conflict set selection in IEEE 802.11 WMNs, in: Proceedings of the 12th ACM Symposium on QoS and Security for Wireless and Mobile Networks (Q2SWinet), Malta, 2016, pp. 103–110.
- 1245 [64] A. Goldsmith, Wireless communications, Cambridge university press, 2005.
- [65] K. Xu, M. Gerla, S. Bae, How effective is the IEEE 802.11 RTS/CTS handshake in ad hoc networks, in: Proceedings of the IEEE Global Telecommunications Conference (GLOBECOM), Taipei, Taiwan, 2002, pp. 72–76.
- 1250 [66] W. C. Anderton, M. Young, Is our model for contention resolution wrong?: Confronting the cost of collisions, in: Proceedings of the 29th ACM Symposium on Parallelism in Algorithms and Architectures, SPAA '17, ACM, Washington, DC, USA, 2017, pp. 183–194.